Faculty of Natural Science and Technology
Department of Physics

◨ NTNU

Norwegian University of
Science and Technology

MASTER'S THESIS
FOR

STUD. TECHN. GAUTE OFTEDAL

Thesis started: [01.20.2009]
Thesis submitted: [06.16.2009]

DISCIPLINE: APPLIED PHYSICS

English title: Towards a DFT-based reactive force field for lead, strontium, titanium, and oxygen.

Norsk tittel: Beregninger med sikte på et DFT-basert reaktivt kraftfelt for bly, strontium, titan og oksygen.

This work has been carried out at the Norwegian University of Science and Technology, under the supervision of associate professor Jon Andreas Støvneng

———————————————————

Trondheim, [01.19.2009]

Jon Andreas Støvneng

Responsible supervisor

Associate professor at the Department of Physics

Preface

This master thesis is written by Gaute Oftedal, as a student in the Program for Applied Physics, Department of Physics, NTNU, Norway. A thank is given to the teaching supervisor, associate professor Jon Andreas Støvneng for guidance with this thesis. Further, a thank is given to NTNU and UIT for sharing CPU time from supercomputers Njord and Stallo, respectively.

Abstract

This study is part of a project with the goal of studying $PbTiO_3$ tetragonal perovskite films grown on $SrTiO_3$ cubic perovskite substrates. This structure can be used in computational storage units since $PbTiO_3$ tetragonal perovskite is ferroelectric at room temperature. In the future, this film-substrate structure will be studied by a reactive force field, ReaxFF, for strontium, oxygen, lead, and titanium. The data set for parametrizing the force field is made by using Amsterdam Density Functional, a program package using Density Functional Theory (DFT) and a Slater-type orbital basis set. The RPBE exchange and correlation functional is used, with zeroth-order regular approximation with spin-orbit coupling to correct for relativistic effects. In this thesis, DFT is used for finding the energy for different lattice constants of 6 crystal structures and the energy of 22 variations in bond lengths, valence angles, and torsion angles of molecules, as these energies are to be added to the data set. Hydrogen atoms were included in many of the molecules to make closed shell systems. A ReaxFF force field for lead, fit against DFT energies for 4 crystal lattices, is made, and compared to those crystals, in addition to two other lead crystals and a Pb_2 molecule. The force field fits well for some of the crystals, e.g. BCC and HCP, but less well for others, e.g. the *cubic diamond* structure and SC. Comparing energies for the Pb_2 molecule shows that the ReaxFF force field binding energy might be weaker than the DFT binding energy. The Pb_2 molecule otherwise demonstrates a good fit to the data set, indicating that the transferability of the ReaxFF force field might be good.

Sammendrag

Denne studien er en del av et prosjekt som har som mål å studere $PbTiO_3$ tetragonal perovskitt filmer grodd på $SrTiO_3$ kubisk perovskitt underlag. Denne strukturen kan bli brukt i lagringsenheter fordi $PbTiO_3$ tetragonal perovskitt er ferroelektrisk i romtemperatur. Denne film-underlag-strukturen vil senere bli studert med et reaktivt kraftfelt, ReaxFF, for strontium, oksygen, bly og titan. Databasen for å parametrisere kraftfeltet er lagd ved å bruke Amsterdam Density Functional, en programpakke som benytter seg av Tetthetsfunksjonalteori (DFT) og bruker Slater-type orbitaler som basissett. En utveksling-og korrelasjonsfunksjonal, RPBE, er brukt, med en nullteordens ordinær tilnærming med spinn-bane-kobling for å korrigere for relativistiske effekter. I denne tésen blir DFT brukt til å finne energien for forskjellige gitterkonstanter til 6 krystallstrukturer og energien til 22 variasjoner i bindingslengder, valensvinkler, og torsjonsvinkler i molekyler, da disse energiene vil bli lagt til databasen. Hydrogenatomer er lagt til molekylene for å lage lukkede skall-systemer. Et ReaxFF kraftfelt for bly, tilpasset DFT energier for 4 krystallgitter, er lagd og sammenlignet med krystallgitterene det ble tilpasset, i tillegg til to andre blykrystaller og et Pb_2-molekyl. Kraftfelt passer bra for noen av krystallene, f.eks. *BCC* og *HCP*, men mindre bra for andre, f.eks. *kubisk diamant* og *SC*. Ved å sammenligne energier for Pb_2-molekylet viser vi at ReaxFF kraftfeltets bindingsenergi kanskje er noe svakere enn bindingsenergien for DFT. Ellers viser det seg at Pb_2-molekylet er godt tilpasset databasen, noe som taler for at overføringsevn til kraftfeltet er god.

Contents

List of Tables

List of Figures

vii

Table 1: Definition of symbols and expressions

Symbols/expressions	Explanation
SC, BCC, FCC, HCP, diamond, cubic $l1_0$ or just $l1_0$, B1, B2, α	Crystal lattices, described in appendix A.
ADF	Amsterdam Density Functional, a program package for calculating molecular and crystal energies and electronic and magnetic properties with DFT.
Data set	A set of data. In this report the data set contains ADF energies, electric properties, and magnetic properties for different geometries, although only ADF energies are used in this report.
Volume/atom or volume/atoms	The volume for a unit cell divided on the number of atoms in that unit cell. For unit cells with two different atoms with a 1 to 1 ratio, the volume/atoms are the volume per those two atoms.
V_0	Volume/atom or volume/atoms when the geometry is optimized.
ReaxFF	A force field developed to be able to describe continuous bond formations and breakings.
Valence angle	The angle between two interatomic bonds a_1-a_2 and a_2-a_3, where a_1, a_2, and a_3 are atoms. The valence angle is also called 'bond angle'.
Torsion angle	The angle between two interatomic bonds a_1-a_2 and a_3-a_4 when the bonds are projected down to the normal plane of the a_2-a_3 bond.
ZORA$_{SR}$, ZORA$_{SO}$	Zeroth-Order Regular Approximation. A method for compensating for relativistic effects in atoms, specially for the most tightly bound electrons in heavy atoms. ZORA$_{SR}$ ZORA$_{SO}$
Å	Ångstrom, $= 10^{-10}$ meters
Gaute force field	A force field made by fitting ReaxFF to data for FCC, HCP, SC, and BCC lead crystals.

1   Introduction

1.1   Research on a PbTiO$_3$ film on a SrTiO$_3$ substrate

Lead titanate (PbTiO$_3$) is ferroelectric for temperatures below 490 °C, having a tetragonal cell structure (the lattice constants $a = b \neq c$) [1]. In Fig. 1, the spontaneous polarizations is along the z axis (up), as the oxygen and titanium atoms are displaced in that direction.
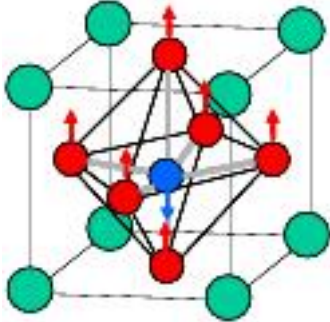
Figure 1: Lead titanate perovskite structure. The lead atoms are placed in the corners while the oxygen atoms are at the sides and the titanium atom is placed in the center. The oxygen atoms are displaced in positive z direction (up) while the titanium atom is displaced in negative z direction.
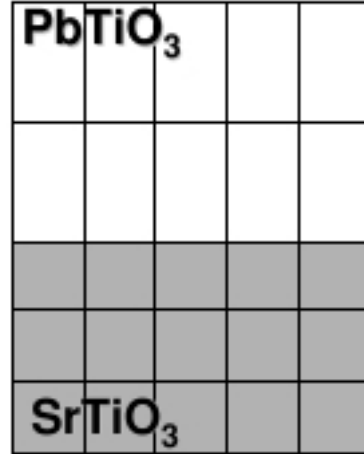
Figure 2: Conventional cross-section TEM sample preparation. The lead titanate crystals are aligned with the quadratic side towards the strontium titanate crystals.

The experimental value for the lattice constant a in SrTiO$_3$ is 3.905 Å [2], while the experimental value for a in PbTiO$_3$ is 3.904 Å and the value for c is 4.150 Å [3]. Both values were measured at room temperature. Because these differences are so small, it is possible to grow a lead titanate film on a strontium titanate surface, getting the lead titanate cells to align as shown in Fig. 2. Because all the cells are aligned in the same direction, a controlled change in the polarization happens when an electric field is applied, making PbTiO$_3$ film on SrTiO$_3$ usable in computational storage units.

1.2   Earlier works on the PbTiO$_3$ film - SrTiO$_3$ substrate

Some experiments on the film-substrate structure have already been conducted, shown in Ref. [4, 5]. T. van Helvoort, B. G. Soleim, R. Holmestad, T. Tybell and Ø. Dahl

have done experiments using a TEM microscope [6]. In TEM, electrons at a spesific wavelength are sent towards a sample material, and some of the electrons are diffracted by the sample and absorbed by a camera or a film on the other side (here, a film). The film used in this experiment was originally dark, but after developing the film, the areas that were hit by electrons were brightened. The experiments gave results such as shown in Fig. 3.
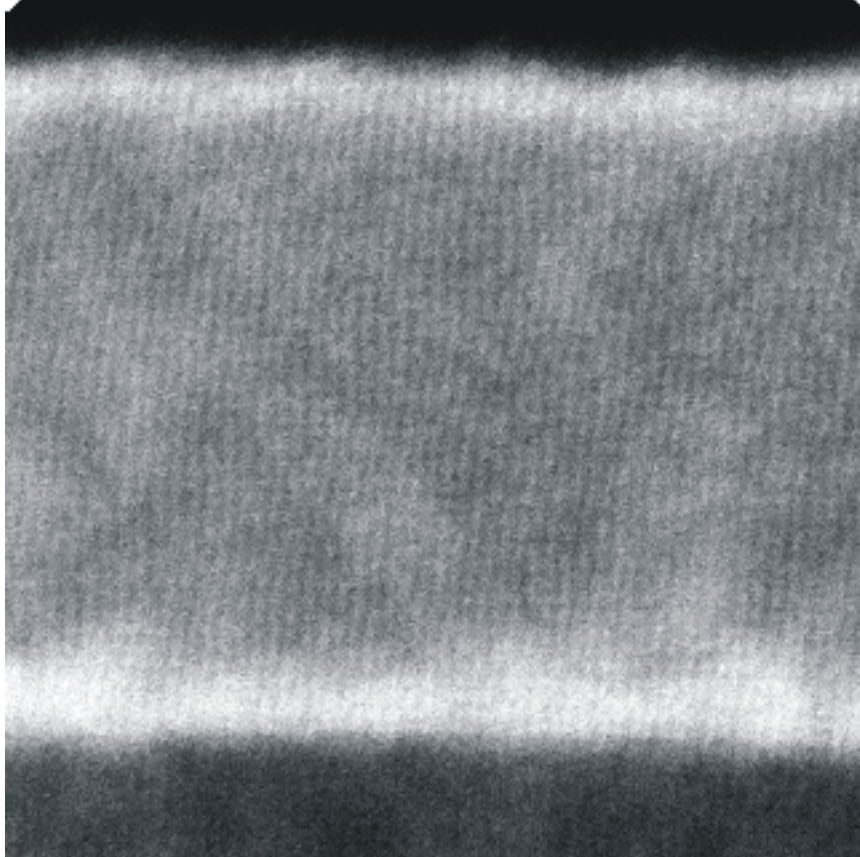
Figure 3: A TEM film showing a PbTiO$_3$ film on a SrTiO$_3$ substrate. The intensity (brightness) shows the density of electrons captured by the film. Lead titanate is the material you see in the middle, covering most of the film, and strontium titanate is the darker material at the bottom. The PbTiO$_3$ film thickness is 191 Å. The increased intensity at the upper film surface is related to an extrinsic effect related to charging of the sample. The increased intensity in the lead titanate film near the strontium titanate surface is not fully understood.

The very bright interface between lead and strontium near the bottom of the figure could not be explained, but some possible reasons have been suggested by the team:

1. Pb deficiency introduced during film growth.

2. Oxygen vacancies in the first layers of the film growth.

3. Static displacements/ distortions in the perovskite structure close to the interface.

4. Strain *out of* the interface plane due to volume conservation or polarization change.

5. Charge accumulation. The film is a ferroelectric with polar structure. Interface charge can arise from polarity discontinuities.

The possibilities 2), 3), 4), and 5) are coupled, as strain and charge are two sides of the same thing in perovskite, oxygen vacancies are coupled to charge and cation displacements. Another important question is: 'What happens to the polarizability when the film thickness is reduced?' Some TEM experiments were also done using very thin films, shown in Fig. 4. The figure shows that the lattice constant ratio c/a is decreased with decreasing film thickness, and the polarizability might cease to exist at some point.
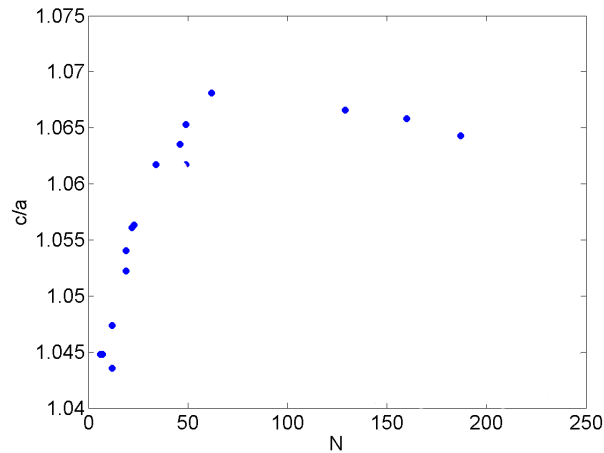
Figure 4: The lattice constant ratio c/a as a function of PbTiO$_3$ thickness. N is the thickness of the film in number of unit cells.

In Ref. [7], ferroelectric behaviour of $PbTiO_3$ film on $SrTiO_3$ substrate has been explored for films only a few unit cells thick, by using simulations fit to first-principles calculations.

1.3 Motivations for this thesis

The most important motivation for this thesis is to work towards making a force field consisting of lead, strontium, oxygen, and titanium parameters. After the force field is finished, one should be able to do different kinds of simulations:

- Simulations to look at lead titanate for different film thicknesses. The polarizability is correlated to the displacement of oxygen and titanium in lead titanate, and it should therefore be possible to say something about what happens to the polarizability for thin films.

- Simulations for looking at film growth on the strontium titanate.

- A more careful study of what happens at and near the lead titanate and strontium titanate interface.

- Studies on other systems, involving some or all of the parametrized atoms.

In addition, the parameters in the force field are transferable to other systems, decreasing the amount of work needed for making another force field containing 1 or more of these atoms. An important point here is, however, that the constants in a force field would vary when fit to different data sets.

1.4 Parameters for a reactive force field with DFT calculations

In this study, we have used DFT (Density Functional Theory) to add data to a data set meant for parametrizing a reactive force field with ReaxFF. DFT can not be used directly to reach the goals as described in section 1.3, as it is a quantum mechanical energy minimization method, and is therefore computationally too expensive for systems containing large numbers of atoms. Earlier studies for adding data to the data set have been conducted for crystals containing lead, strontium, oxygen, and titanium [8, 9]. Those studies have not produced results for crystals consisting of any of these combinations: Lead and strontium, strontium and oxygen, and strontium and titanium crystals. Another study is being conducted parallel to this one by K. T. Olsen [10]. We and K. T. Olsen have found data for lacking crystal structures. In addition, data for *molecules* consisting of strontium, lead, oxygen and titanium

have been found in both studies, as values for molecules are necessary for making a good force field. The process of finding data is described in detail in sections 4.1 and 4.2.

1.5 Making a ReaxFF force field for lead, using lead crystal parameters

In addition to finding data for the reactive force field to be fit against, some work has been done to produce a reactive force field for lead, using the crystal structure data from Ref. [9]. This process is described in section 4.4.

2 Theory

2.1 ReaxFF [11]

ReaxFF is a force field developed by Adri van Duin, William A. Goddard III, and co-workers at the California Institute of Technology. Traditional force fields describe molecular or condensed phase systems by simple harmonic equations that describe the streching and compression of bonds and the bending of valence angles, and add van der Waals potential functions and Coulomb interactions to describe non-bonded interactions. However, harmonic equations for the streching and compression of bonds only hold near the energy equilibrium. Traditional force fields therefore only work for describing systems where interatomic distances and valence angles are close to the energy equilibriumn, as these force fields are unable to model continuous bond formations and breakings. ReaxFF is a better tool for this, as all valence terms (bonds, valence angles, and torsion angles) are dependent on the bond order between atoms, and this bond order is determined uniquely from the interatomic distances. The bond order goes towards zero when these distances become large. Another feature of ReaxFF is that instead of finding constants that match the input data set, it finds more fundamental constants, transferable to other systems. ReaxFF is composed of different energy terms, written as

$$
\begin{aligned}
E_{system} = & E_{bond} + E_{lp} + E_{over} + E_{under} + E_{val} + E_{coa} + E_{tors} + E_{conj} + E_{Hbond} \\
& + E_{C2} + E_{triple} + E_{vdWaals} + E_{Coulomb}
\end{aligned}
\tag{1}
$$

In the following, we will look at each energy term. The constants in the different terms are displayed in table 2. These constants vary for each atom/ atom combination used in the force field, and are found by fitting the constants in ReaxFF to experimental data or computer simulation data. How this is done is explained in some detail in section 2.2.

Table 2: Constants used in the energy terms in ReaxFF.

Parameter	Description	Parameter	Description
r_σ	σ reference bond length	r_π	π reference bond length
$r_{\pi\pi}$	$\pi\pi$ reference bond length	val_i^e	# of valences electrons of atom i
$p_{bo,1}$	bond order parameter	$p_{bo,2}$	bond order parameter
$p_{bo,3}$	bond order parameter	$p_{bo,4}$	bond order parameter
$p_{bo,5}$	bond order parameter	$p_{bo,6}$	bond order parameter
p_{boc1}	BO correction param	p_{boc2}	BO correction param
p_{boc3}	BO correction param	p_{boc4}	BO correction param
p_{boc5}	BO correction param	$p_{be,1}$	bond energy param
$p_{be,2}$	bond energy param	D_e^σ	σ bond energy param
D_e^π	π bond energy param	$D_e^{\pi\pi}$	$\pi\pi$ bond energy param
p_{lp1}	lone pair parameter	p_{lp2}	lone pair parameter
$n_{lp,opt}$	optimal nr. of lone pairs	p_{val1}	valence angle param
p_{val2}	valence angle param	p_{val3}	valence angle param
p_{val4}	valence angle param	p_{val5}	valence angle param
p_{val6}	valence angle param	p_{val7}	valence angle param
p_{val8}	valence angle param	p_{val9}	valence angle param
p_{val10}	valence angle param	p_{val11}	valence angle param
p_{val12}	valence angle param	p_{val13}	valence angle param
p_{val14}	valence angle param	p_{3con1}	3-body conjugation param
p_{3con2}	3-body conjugation param	p_{3con3}	3-body conjugation param
p_{3con4}	3-body conjugation param	p_{tor1}	torsion parameter
p_{tor2}	torsion parameter	p_{4con1}	4-body conjugation param
p_{4con2}	4-body conjugation param	p_{hb1}	hydrogen bond param
p_{hb2}	hydrogen bond param	p_{hb3}	hydrogen bond param
p_c	carbon triple bond param	p_{trip1}	carbon-oxygen param
p_{trip2}	carbon-oxygen param	p_{trip3}	carbon-oxygen param
p_{trip4}	carbon-oxygen param	p_{ovun1}	atom over/underb. param
p_{ovun2}	atom over/underb. param	p_{ovun3}	atom over/underb. param
p_{ovun4}	atom over/underb. param	p_{ovun5}	atom over/underb. param
p_{ovun6}	atom over/underb. param	p_{ovun7}	atom over/underb. param
p_{ovun8}	atom over/underb. param	$\Theta_{0,0}$	valence angle param
V_1	torsion parameter	V_2	torsion parameter
V_3	torsion parameter	R_{cut}	Taper cutoff radius
p_{vdW}	vdW parameter	α_{ij}	vdW parameter
γ_w	vdW parameter	D_{ij}	vdW parameter
γ_{ij}	Coulomb parameter	C	Coulomb parameter

2.1.1 Bond Order (BO) and bond energy

ReaxFF describes continuous bond formation and breaking by using a function for the bond order between any two atoms i and j. The uncorrected bond order, BO_{ij}^{unc}, is shown in eq. 2.

$$
\begin{aligned}
BO_{ij}^{unc} &= BO_{ij}^{unc,\sigma} + BO_{ij}^{unc,\pi} + BO_{ij}^{unc,\pi\pi} \\
&= \exp\left(p_{bo,1}\left(\frac{r_{ij}}{r_\sigma}\right)^{p_{bo,2}}\right) + \exp\left(p_{bo,3}\left(\frac{r_{ij}}{r_\pi}\right)^{p_{bo,4}}\right) + \exp\left(p_{bo,5}\left(\frac{r_{ij}}{r_{\pi\pi}}\right)^{p_{bo,6}}\right)
\end{aligned}
$$
(2)

Here, r_σ, r_π, and $r_{\pi\pi}$ are the reference lengths for the bonds, and $p_{bo,1}$, $p_{bo,3}$, $p_{bo,5}$ are less than 0, making the terms disappear for large r_{ij}s. The constants $p_{bo,2}$, $p_{bo,4}$, and $p_{bo,6}$ are greater than 0. The three bond terms vary from 1 (for low r_{ij} values) to 0 (for high r_{ij} values). Only the σ term is used for bonds involving 1 or 2 atoms with only 1 valence, giving a maximum bond order of 1. For bonds between atoms with only two valences, only the σ term and the π term are used, giving a maximum bond order of 2. The total bond order for an atom should be equal to the number of valences electrons of that atom. This is often not the case, and therefore the uncorrected bond order terms are corrected by introducing some multipliers.

$$
\begin{aligned}
BO_{ij}^\sigma &= BO_{ij}^{unc,\sigma} f_1(\Delta_i^{unc}, \Delta_j^{unc}) f_4(\Delta_i^{unc}, BO_{ij}^{unc}) f_5(\Delta_j^{unc}, BO_{ij}^{unc}) \\
BO_{ij}^\pi &= BO_{ij}^{unc,\pi} \left[f_1(\Delta_i^{unc}, \Delta_j^{unc})\right]^2 f_4(\Delta_i^{unc}, BO_{ij}^{unc}) f_5(\Delta_j^{unc}, BO_{ij}^{unc}) \\
BO_{ij}^{\pi\pi} &= BO_{ij}^{unc,\pi\pi} \left[f_1(\Delta_i^{unc}, \Delta_j^{unc})\right]^2 f_4(\Delta_i^{unc}, BO_{ij}^{unc}) f_5(\Delta_j^{unc}, BO_{ij}^{unc}) \\
BO_{ij} &= BO_{ij}^\sigma + BO_{ij}^\pi + BO_{ij}^{\pi\pi}
\end{aligned}
$$
(3)

$$
\begin{aligned}
f_1(\Delta_i^{unc}, \Delta_j^{unc}) &= \frac{1}{2}\frac{val_i + f_2(\Delta_i^{unc}, \Delta_j^{unc})}{val_i + f_2(\Delta_i^{unc}, \Delta_j^{unc}) + f_3(\Delta_i^{unc}, \Delta_j^{unc})} \\
&+ \frac{1}{2}\frac{val_j + f_2(\Delta_i^{unc}, \Delta_j^{unc})}{val_j + f_2(\Delta_i^{unc}, \Delta_j^{unc}) + f_3(\Delta_i^{unc}, \Delta_j^{unc})}
\end{aligned}
$$
(4)

$$
f_2(\Delta_i^{unc}, \Delta_j^{unc}) = \exp(-p_{boc1}\Delta_i^{unc}) + \exp(-p_{boc1}\Delta_j^{unc})
$$
(5)

$$
f_3(\Delta_i^{unc}, \Delta_j^{unc}) = \frac{1}{p_{boc2}}\ln\left(\frac{1}{2}[\exp(-p_{boc2}\Delta_i^{unc}) + \exp(-p_{boc2}\Delta_j^{unc})]\right)
$$
(6)

$$
f_4(\Delta_i^{unc}, BO_{ij}^{unc}) = \left[1 + \exp(-p_{boc3}[p_{boc4}BO_{ij}^{unc}BO_{ij}^{unc} - \Delta_i^{unc}] + p_{boc5})\right]^{-1}
$$
(7)

$$
f_5(\Delta_j^{unc}, BO_{ij}^{unc}) = \left[1 + \exp(-p_{boc3}[p_{boc4}BO_{ij}^{unc}BO_{ij}^{unc} - \Delta_j^{unc}] + p_{boc5})\right]^{-1}
$$
(8)

9

The valences of atom i is denoted as val_i (as an example 4 for carbon, 1 for hydrogen). The degree of deviation for the sum of the corrected bond orders around an atomic center denoted from it's atomic center, Δ_i, is

$$\Delta_i = \sum_{j=1}^{neighbours(i)} BO_{ij} - val_i \tag{9}$$

The energy, E_{bond}, is due to the interatomic distance between a pair of atoms, and is given as

$$E_{bond} = -D_e^\sigma BO_{ij}^\sigma \exp(p_{be,1}[1 - (BO_{ij}^\sigma)^{p_{be,2}}]) - D_e^\pi BO_{ij}^\pi - D_e^{\pi\pi} BO_{ij}^{\pi\pi} \tag{10}$$

2.1.2 Lone pair energy

Eq. (11) is used to determine the number of lone pairs around an atom. The "int" operator rounds the number down to nearest integer.

$$n_{lp,i} = \text{int}\left(\frac{\Delta_i^e}{2}\right) + \exp\left(-p_{lp1}\left[2 + \Delta_i^e - 2\text{int}\left(\frac{\Delta_i^e}{2}\right)\right]^2\right) \tag{11}$$

In (12), Δ_i^e is determined. It describes the difference between the total number of outer shell electrons, val_i^e and the sum of bond orders around an atom i.

$$\Delta_i^e = val_i^e - \sum_{j=1}^{neighbours(i)} BO_{ij} \tag{12}$$

For oxygen with normal coordination, (11) leads to 2 lone pairs. Oxygen has six electrons in the outer shell, and the preferred bond order for oxygen is 2. Because Δ_i^e is 4, $\text{int}(\Delta_i^e/2)$ is 2, and the exponential is very small, meaning $n_{lp,i} \approx 2$. As the total bond order associated with a particular oxygen atom starts to exceed 2, (11) causes a lone pair to gradually break up, causing a deviation Δ_i^{lp}, defined in (13), from the optimal number of lone pairs $n_{lp,opt}$ (2 for oxygen, 0 for silicon and hydrogen).

$$\Delta_i^{lp} = n_{lp,opt} - n_{lp,i} \tag{13}$$

This is accompanied by an energy penalty, as calculated in (14).

$$E_{lp} = \frac{p_{lp2}\Delta_i^{lp}}{1 + \exp(-75\Delta_i^{lp})} \tag{14}$$

2.1.3 Atom under-/overcoordination

Even after correction of the original bond orders BO_{ij}^{unc}, a degree of overcoordination ($\Delta_i > 0$) may remain in the molecule. The overcoordination term has been added to handle this error. The overcoordination term is given as

$$E_{over} = \frac{\sum_{j=1}^{n} p_{ovun1} D_e^{\sigma} BO_{ij}}{\Delta_i^{lpcorr} + val_i} \Delta_i^{lpcorr} (1 + \exp[p_{ovun2}\Delta_i^{lpcorr}])^{-1} \tag{15}$$

$$\Delta_i^{lpcorr} = \Delta_i - \frac{\Delta_i^{lp}}{1 + p_{ovun3} \exp\left(p_{ovun4}\left[\sum_{j=1}^{neighbours(i)}(\Delta_j - \Delta_j^{lp})(BO_{ij}^{\pi} + BO_{ij}^{\pi\pi})\right]\right)} \tag{16}$$

For an undercoordinated atom ($\Delta_i < 0$), the energy contribution for the resonance of the π-electron between attached under-coordinated atomic centers is taken into account. This is done in (17). E_{under} is only important if the bonds between undercoordinated atoms partly have π-bond character.

$$E_{under} = -p_{ovun5}\frac{1 - \exp(p_{ovun6}\Delta_i^{lpcorr})}{1 + \exp(-p_{ovun2}\Delta_i^{lpcorr})}$$

$$\cdot \left(1 + p_{ovun7} \exp\left[p_{ovun8}\left(\sum_{j=1}^{neightbours(i)}\left[\Delta_j - \Delta_j^{lp}\right][BO_{ij}^{\pi} + BO_{ij}^{\pi\pi}]\right)\right]\right)^{-1} \tag{17}$$

2.1.4 Valence angle

The valence angle energy for valence angle i-j-k, where i, j, and k are locations for 3 atoms, is

$$E_{val} = f_7(BO_{ij})f_7(BO_{jk})f_8(\Delta_j)(p_{val1} - p_{val1}\exp[-p_{val2}(\Theta_0(BO) - \Theta_{ijk})^2]) \tag{18}$$

$$f_7(BO_{ij}) = 1 - \exp(-p_{val3}BO_{ij}^{p_{val4}}) \tag{19}$$

$$f_8(\Delta_j) = p_{val5} - (p_{val5} - 1)\frac{2 + \exp(p_{val6}\Delta_j^{angle})}{1 + \exp(p_{val6}\Delta_j^{angle}) + \exp(-p_{val7}\Delta_j^{angle})} \tag{20}$$

$$SBO = \sum_{n=1}^{neighbours(j)} (BO_{jn}^{\pi} + BO_{jn}^{\pi\pi})$$

$$+ \left(1 - \prod_{n=1}^{neighbours(j)} \exp[-BO_{jn}]\right)(-\Delta_j^{angle} - p_{val8}n_{lp,j}) \tag{21}$$

11

$$\Delta_j^{angle} = -val_j + \sum_{n=1}^{neighbours(j)} BO_{jn} \tag{22}$$

$$
\begin{aligned}
SBO2 &= 0 \text{ if } SBO \leq 0 \\
SBO2 &= SBO^{p_{val9}} \text{ if } 0 < SBO < 1 \\
SBO2 &= 2 - (2 - SBO)^{p_{val9}} \text{ if } 1 < SBO < 2 \\
SBO2 &= 2 \text{ if } SBO > 2
\end{aligned}
$$

$$\tag{23}$$

$$\Theta_0(BO) = \pi - \Theta_{0,0}(1 - \exp[-\lambda_{18}(2 - SBO2)]) \tag{24}$$

Eq. 18 is the calculated energy associated with deviations in valence angle Θ_{ijk} from its equilibrium value Θ_0. Eq. 19 describes $f_7(BO_{ij})$, that is a term that ensures that the angle energy disappears smoothly if one of the two bonds in the angle breaks. Eq. 20 deals with the over/undercoordination in the central atom j on the valence angle energy. Eq. 21 shows the equilibrium angle Θ_0 around the central atom j, as the angle is dependent on the order of π - bonds between j and the two atoms it is bound to. To reproduce the stability of systems with two double bonds sharing an atom in a valence angle, an additional energy penalty has to be accounted for, shown in eq. 25 and eq. 26.

$$E_{pen} = p_{val11} f_9(\Delta_j) \exp(-p_{val12}[BO_{ij} - 2]^2) \exp(-p_{val12}[BO_{jk} - 2]^2) \tag{25}$$

$$\frac{2 + \exp(-p_{val13}\Delta_j)}{1 + \exp(-p_{val13}\Delta_j) + \exp(p_{val14}\Delta_j)} \tag{26}$$

2.1.5   Three body conjugation term

The three-body conjugation energy is given in (27)

$$
E_{coa} = p_{3con1}(1 + \exp[p_{3con2}\Delta_j^{val}])^{-1} \exp\left(-p_{3con3}\left[-BO_{ij} + \sum_{n=1}^{neighbours(i)} BO_{in}\right]^2\right)
$$

$$
\cdot \exp\left(-p_{3con3}\left[-BO_{jk} + \sum_{n=1}^{neighbours(i)} BO_{kn}\right]^2\right)
$$

$$
\cdot \exp(-p_{3con4}[BO_{ij} - 1.5]^2) \exp(-p_{3con4}[BO_{jk} - 1.5]^2)
$$

$$\tag{27}$$

2.1.6 Torsion angle energy

The torsion energy is described in eq. 28. The equations give a good description of what happens when the BO $\rightarrow$ 0 and when the BO is greater than 1. The $\sin(\Theta_{ijk})\sin(\Theta_{jkl})$ term in eq. 28 ensures that the torsion energy disappears when one of the valence angles approaches π. Eq. 29 describes a smooth disappearance of the torsion energy when one of the bonds in the torsion angle breaks. The torsion angle is denoted as ω_{ijkl}.

$$
\begin{aligned}
E_{tors} = {} & f_{10}(BO_{ij}, BO_{jk}, BO_{kl})\sin\Theta_{ijk}\sin\Theta_{jkl} \\
& \cdot [\frac{1}{2}V_1(1 + \cos\omega_{ijkl}) \\
& + \frac{1}{2}V_2\exp[p_{tor1}(BO_{jk} - 1 + f_{11}(\Delta_j, \Delta_k))^2](1 - \cos 2\omega_{ijkl}) \\
& + \frac{1}{2}V_3(1 + \cos 3\omega_{ijkl})]
\end{aligned}
\tag{28}
$$

$$
\begin{aligned}
f_{10}(BO_{ij}, BO_{jk}, BO_{kl}) = {} & (1 - \exp[-p_{tor2}BO_{ij}]) \\
& \cdot (1 - \exp[-p_{tor2}BO_{jk}])(1 - \exp[-p_{tor2}BO_{kl}])
\end{aligned}
\tag{29}
$$

2.1.7 Four body conjugation term

This is the energy contribution of conjugation effects in the moleculecular energy for four atoms. A maximum contribution of conjugation energy is obtained when successive bonds have bond order values of 1.5. The energy is given in eq. 30 and 31:

$$
E_{conj} = f_{11}(BO_{ij}, BO_{jk}, BO_{kl})p_{4con1}(1 + [\cos^2\omega_{ijkl} - 1]\sin\Theta_{ijk}\sin\Theta_{jkl})
\tag{30}
$$

$$
\begin{aligned}
f_{11}(BO_{ij}, BO_{jk}, BOkl) = {} & \exp\left(-p_{4con2}\left[BO_{ij} - \frac{1}{2}\right]^2\right) \\
& \cdot \exp\left(-p_{4con2}\left[BO_{jk} - \frac{1}{2}\right]^2\right)\exp\left(-p_{4con2}\left[BO_{kl} - \frac{1}{2}\right]^2\right)
\end{aligned}
\tag{31}
$$

2.1.8 Hydrogen bond interactions

In eq. 32 the bond-order dependent hydrogen bond term for a X-H $-$ Z system is described, where X and Z are random atoms, and H is a hydrogen atom.

$$
E_{Hbond} = p_{hb1}(1 - \exp[p_{hb2}BO_{XH}])\exp\left(p_{hb3}\left[\frac{r^0_{hb}}{r_{HZ}} + \frac{r_{HZ}}{r^0_{hb}} - 2\right]\right)\sin^8\left(\frac{\theta_{XHZ}}{2}\right)
\tag{32}
$$

The distance between atom X and the hydrogen atom at equilibrium is r_{hb}^0, while r_{HZ} is the distance between the hydrogen atom and atom Z.

2.1.9 Correction for C_2

A correction for a too strong triple bond between two carbon atoms is shown in eq. 33.

$$
\begin{aligned}
E_{C2} &= p_c(BO_{ij} - \Delta_i - 0.04\Delta_i^4 - 3)^2 \text{ if } BO_{ij} - \Delta_i - 0.04\Delta_i^4 > 3 \\
E_{C2} &= 0 \text{ if } BO_{ij} - \Delta_i - 0.04\Delta_i^4 \leq 3
\end{aligned} \tag{33}
$$

2.1.10 Carbon-oxygen triple bond energy correction

To better describe the triple bond in carbon monoxide the energy correction in eq. 34 is used.

$$
\begin{aligned}
E_{trip1} = {} & p_{trip1} \exp(-p_{trip2}[BO_{ij} - 2.5]^2) \\
& \cdot \frac{\exp\left(-p_{trip4}\left[\sum_{k=1}^{neighbours(i)} BO_{ik} - BO_{ij}\right]\right)}{1 + 25\exp(p_{trip3}[\Delta_i + \Delta_j])} \\
& + \frac{\exp\left(-p_{trip4}\left[\sum_{k=1}^{neighbours(i)} BO_{jk} - BO_{ij}\right]\right)}{1 + 25\exp(p_{trip3}[\Delta_i + \Delta_j])}
\end{aligned} \tag{34}
$$

2.1.11 Taper correction

In addition to valence interactions which depend on overlap, there are repulsive interactions at short interatomic distances due to the Pauli principle, and attraction energies at long distances due to dispersion. These interactions are van der Waals and Coulomb forces, and are included for *all* atom pairs. To avoid energy discontinuities when charges move in and out of the non-bonded cutoff radius, ReaxFF employs a Taper correction, developed by de Vos Burchart (1995). Each nonbonded energy and derivative is multiplied by a Taper-term, which is taken from a distance-dependent 7th order polynomial (35).

$$
Tap = Tap_7 r_{ij}^7 + Tap_6 r_{ij}^6 + Tap_5 r_{ij}^5 + Tap_4 r_{ij}^4 + Tap_3 r_{ij}^3 + Tap_2 r_{ij}^2 + Tap_1 r_{ij} + Tap_0 \tag{35}
$$

The terms in this polynomial are chosen to ensure that all 1st, 2nd, and 3rd derivatives of the nonbonded interactions to the distance are continuous and go to zero at the cutoff boundary. To that end, the terms Tap_0 to Tap_7 in (35) are calculated in (36),

where R_{cut} is the non-bonded cutoff radius.

$$
\begin{aligned}
Tap_7 &= 20/R_{cut}^7 \\
Tap_6 &= -70/R_{cut}^6 \\
Tap_5 &= 84/R_{cut}^5 \\
Tap_4 &= -35/R_{cut}^4 \\
Tap_3 &= 0 \\
Tap_2 &= 0 \\
Tap_1 &= 0 \\
Tap_0 &= 1
\end{aligned}
\tag{36}
$$

2.1.12 van der Waals interactions

One uses a distance-corrected Morse-potential for the van der Waals interaction, shown in eq 37. To avoid an excessively high repulsion between bonded atoms and atoms sharing a valence angle, a shielded interaction, eq. 38, is included in the equation.

$$
E_{vdWaals} = Tap \cdot D_{ij} \left(\exp\left[\alpha_{ij}\left(1 - \frac{f_{12}(r_{ij})}{r_{vdW}}\right)\right] - 2\exp\left[\frac{1}{2}\alpha_{ij}\left(1 - \frac{f_{12}(r_{ij})}{r_{vdW}}\right)\right]\right)
\tag{37}
$$

$$
f_{12}(r_{ij}) = \left(r_{ij}^{p_{vdW}} + \left[\frac{1}{\gamma_w}\right]^{p_{vdW}}\right)^{1/p_{vdW}}
\tag{38}
$$

2.1.13 Coulomb interactions

As with van der Waals interactions, this interaction is between all atom pairs. To adjust for orbital overlap between atoms at close distances, a shielded Coulomb-potential is used (39).

$$
E_{Coulomb} = Tap \cdot C \frac{q_i q_j}{(r_{ij}^3 + [1/\gamma_{ij}]^3)^{1/3}}
\tag{39}
$$

The atomic charges, q_i and q_j, are calculated using the Electron Equilibration Method [12, 13].

2.2 ReaxFF software

The recipe for making a force field using ReaxFF software is described in this section. The files important for this study are described here, although more are included in the software. The file names and a short description of each file are shown in table 3.

Table 3: Overview of ReaxFF input files used in this study.

File name	Short description
geo	the geometries for the system
ffield	the force field constants
trainset.in	the data set with weighting
params	optimizable force field parameters
fort.4	the force field output
fort.99	the file displaying the error

2.2.1   geo

The geo file describes the geometries for the system, both for crystals and molecules. The file is divided into blocks, where each block describes one geometry, and is identified in the DESCRP line. An example of a block is shown in Fig. 5, using an FCC lead structure.

```
XTLGRF 200
DESCRP pb_fcc_5.18
REMARK Pb fcc structure at energy minimum, a = 5.18 AA
CRYSTX    5.18000    5.18000    5.18000   90.00000   90.00000   90.00000
HETATM    1 Pb              0.00000    0.00000    0.00000
HETATM    2 Pb              0.00000    2.59000    2.59000
HETATM    3 Pb              2.59000    2.59000    0.00000
HETATM    4 Pb              2.59000    0.00000    2.59000
UNIT ENERGY   kcal
ENERGY          -307.40
END

XTLGRF 200
DESCRP pb_fcc_3.99
REMARK Pb fcc structure at a = 3.99 AA
CRYSTX    3.99000    3.99000    3.99000   90.00000   90.00000   90.00000
HETATM    1 Pb              0.00000    0.00000    0.00000
HETATM    2 Pb              0.00000    1.99500    1.99500
HETATM    3 Pb              1.99500    1.99500    0.00000
HETATM    4 Pb              1.99500    0.00000    1.99500
UNIT ENERGY   kcal
ENERGY            89.72
END
```

Figure 5: A geo example file showing two blocks of FCC with different lattice constants. The first line of a block tells ReaxFF what format is used for that block. The DESCRP line works as an identifier for that block, so that the block can be identified with parameters in the trainset.in file. The three first numbers in the CRYSTX line are the lengths of the three lattice vectors, and the three last numbers are the angles between these vectors. Each HETATM line describes the basis vector in cartesian coordinates for each atom in the lattice cell. The other lines are different kinds of remarks, not necessary to the geo file.

2.2.2   ffield

This file contains all constants used in the force field. A rough overview of these constants is given in Fig. 2.

2.2.3   trainset.in

This file contains all data in the data set except for the molecule/crystal geometries. As this study only focuses on making a force field for lead, using lead crystals, there are no polarizations, so the only block in trainset.in is the energy block. An example of this file is shown in Fig. 6.

17

```
ENERGY
# equilibrium energy differences
0.05   + pb_fcc_5.18/4 - pb_hcp_3.55/2   -0.03
0.05   + pb_fcc_5.18/4 - pb_sc_3.37/1    -2.64
0.5    + pb_fcc_5.18/4 - pb_d_7.27/8     -2.78
0.05   + pb_fcc_5.18/4 - pb_bcc_4.10/2   -0.69
# bcc
2.0  + pb_bcc_4.10/2 - pb_bcc_3.20/2   -85.49
1.0  + pb_bcc_4.10/2 - pb_bcc_3.40/2   -39.95
1.0  + pb_bcc_4.10/2 - pb_bcc_3.58/2   -17.70
1.0  + pb_bcc_4.10/2 - pb_bcc_3.74/2   -7.12
1.0  + pb_bcc_4.10/2 - pb_bcc_3.89/2   -2.02
1.0  + pb_bcc_4.10/2 - pb_bcc_4.16/2   -0.35
1.0  + pb_bcc_4.10/2 - pb_bcc_4.28/2   -1.29
1.0  + pb_bcc_4.10/2 - pb_bcc_4.40/2   -2.77
0.4  + pb_bcc_4.10/2 - pb_bcc_4.51/2   -4.72
0.2  + pb_bcc_4.10/2 - pb_bcc_4.61/2   -6.52
# sc
2.0  + pb_sc_3.37/1  - pb_sc_2.61/1   -83.40
1.0  + pb_sc_3.37/1  - pb_sc_2.77/1   -39.39
1.0  + pb_sc_3.37/1  - pb_sc_2.92/1   -17.28
1.0  + pb_sc_3.37/1  - pb_sc_3.05/1   -6.96
1.0  + pb_sc_3.37/1  - pb_sc_3.18/1   -1.91
1.0  + pb_sc_3.37/1  - pb_sc_3.40/1   -0.22
1.0  + pb_sc_3.37/1  - pb_sc_3.50/1   -1.19
1.0  + pb_sc_3.37/1  - pb_sc_3.59/1   -2.50
0.4  + pb_sc_3.37/1  - pb_sc_3.68/1   -4.12
0.2  + pb_sc_3.37/1  - pb_sc_3.77/1   -6.07
# diamond
2.0  + pb_d_7.27/8   - pb_d_5.67/8   -75.09
1.0  + pb_d_7.27/8   - pb_d_6.02/8   -35.31
1.0  + pb_d_7.27/8   - pb_d_6.34/8   -15.67
1.0  + pb_d_7.27/8   - pb_d_6.63/8   -6.18
1.0  + pb_d_7.27/8   - pb_d_6.89/8   -1.81
1.0  + pb_d_7.27/8   - pb_d_7.37/8   -0.22
1.0  + pb_d_7.27/8   - pb_d_7.59/8   -0.89
1.0  + pb_d_7.27/8   - pb_d_7.79/8   -2.22
0.4  + pb_d_7.27/8   - pb_d_7.99/8   -3.76
0.2  + pb_d_7.27/8   - pb_d_8.17/8   -5.47
ENDENERGY
```

Figure 6: A data set file when using lead crystals. In the second and third column, one crystal structure is substracted from another. The energy is per atom, so each crystal structure is divided by the number of atoms in the unit cell. The fourth line is the energy, here in kcal/mol, found experimentally or by computations. The numbers in the first column are the weighting of each energy comparison, the importance of the comparison is $1/\text{weight}^2$.

The energy in the trainset.in file is here the energy difference between two crystal structures from the geo file. In this file, one also decides the weight for each of these energies.

2.2.4 fort.99

The error is displayed in the fort.99 file, and is a measurement of the difference between the ReaxFF force field and the data set for a given geometry. When only using energy differences as parameters in trainset.in, the error is found by (40).

$$ERROR = ([ffieldenergy - trainsetvalue]/weight)^2 \qquad (40)$$

Here, $trainsetvalue$ is the energy defined in the trainset.in file, and $ffieldenergy$ is the corresponding energy calculated by the current force field. The total error of the force field is the sum of all $ERROR$s, one $ERROR$ for each line in the trainset.in file. An example of a fort.99 file is shown in Fig. 7.

```
                              FFiled value QM/Lit value  Weight      Error   Total error
Energy +pb_fcc_5.18/  4 -pb_hcp_3.55/  2    -0.7168      -0.0300     0.0500   188.6577      188.6577
Energy +pb_fcc_5.18/  4 -pb_sc_3.37/   1    -2.1990      -2.6400     0.0500    77.7855      266.4432
Energy +pb_fcc_5.18/  4 -pb_d_7.27/    8    -5.5333      -2.7800     0.5000    30.3233      296.7665
Energy +pb_fcc_5.18/  4 -pb_bcc_4.10/  2    -0.3316      -0.6900     0.0500    51.3935      348.1599
Energy +pb_bcc_4.10/  2 -pb_bcc_3.20/  2   -68.1793     -85.4900     2.0000    74.9147      423.0746
Energy +pb_bcc_4.10/  2 -pb_bcc_3.40/  2   -29.3991     -39.9500     1.0000   111.3206      534.3953
Energy +pb_bcc_4.10/  2 -pb_bcc_3.58/  2   -12.7864     -17.7000     1.0000    24.1431      558.5384
Energy +pb_bcc_4.10/  2 -pb_bcc_3.74/  2    -5.4777      -7.1200     1.0000     2.6971      561.2355
Energy +pb_bcc_4.10/  2 -pb_bcc_3.89/  2    -2.0237      -2.0200     1.0000     0.0000      561.2355
Energy +pb_bcc_4.10/  2 -pb_bcc_4.16/  2     0.2458      -0.3500     1.0000     0.3550      561.5905
Energy +pb_bcc_4.10/  2 -pb_bcc_4.28/  2     0.4920      -1.2900     1.0000     3.1753      564.7659
Energy +pb_bcc_4.10/  2 -pb_bcc_4.40/  2     0.5322      -2.7700     1.0000    10.9042      575.6701
Energy +pb_bcc_4.10/  2 -pb_bcc_4.51/  2     0.4709      -4.7200     0.4000   168.4074      744.0776
Energy +pb_bcc_4.10/  2 -pb_bcc_4.61/  2     0.3739      -6.5200     0.2000  1188.1587     1932.2363
Energy +pb_fcc_5.18/  4 -pb_fcc_3.99/  4   -75.1693     -99.2800     2.0000   145.3314     2077.5677
Energy +pb_fcc_5.18/  4 -pb_fcc_4.24/  4   -32.4247     -47.2000     1.0000   218.3084     2295.8760
Energy +pb_fcc_5.18/  4 -pb_fcc_4.47/  4   -13.9425     -21.1600     1.0000    52.0921     2347.9682
Energy +pb_fcc_5.18/  4 -pb_fcc_4.67/  4    -6.0751      -8.8900     1.0000     7.9239     2355.8921
Energy +pb_fcc_5.18/  4 -pb_fcc_4.87/  4    -2.2042      -2.8800     1.0000     0.4568     2356.3488
Energy +pb_fcc_5.18/  4 -pb_fcc_5.19/  4     0.0292      -0.0300     1.0000     0.0035     2356.3523
Energy +pb_fcc_5.18/  4 -pb_fcc_5.35/  4     0.2999      -1.0200     1.0000     1.7421     2358.0944
Energy +pb_fcc_5.18/  4 -pb_fcc_5.49/  4     0.3301      -2.4600     1.0000     7.7848     2365.8792
Energy +pb_fcc_5.18/  4 -pb_fcc_5.63/  4     0.2569      -4.1000     0.4000   118.6423     2484.5215
Energy +pb_fcc_5.18/  4 -pb_fcc_5.76/  4     0.1423      -6.2200     0.2000  1011.9712     3496.4926
Energy +pb_sc_3.37/   1 -pb_sc_2.61/   1   -83.7115     -83.4000     2.0000     0.0243     3496.5169
Energy +pb_sc_3.37/   1 -pb_sc_2.77/   1   -44.7737     -39.3900     1.0000    28.9841     3525.5010
Energy +pb_sc_3.37/   1 -pb_sc_2.92/   1   -21.2511     -17.2800     1.0000    15.7699     3541.2708
Energy +pb_sc_3.37/   1 -pb_sc_3.05/   1   -10.2394      -6.9600     1.0000    10.7547     3552.0255
Energy +pb_sc_3.37/   1 -pb_sc_3.18/   1    -4.1649      -1.9100     1.0000     5.0846     3557.1102
Energy +pb_sc_3.37/   1 -pb_sc_3.40/   1     0.3571      -0.2200     1.0000     0.3331     3557.4432
Energy +pb_sc_3.37/   1 -pb_sc_3.50/   1     1.1894      -1.1900     1.0000     5.6615     3563.1047
Energy +pb_sc_3.37/   1 -pb_sc_3.59/   1     1.6023      -2.5000     1.0000    16.8285     3579.9333
Energy +pb_sc_3.37/   1 -pb_sc_3.68/   1     1.8135      -4.1200     0.4000   220.0384     3799.9717
Energy +pb_sc_3.37/   1 -pb_sc_3.77/   1     1.8978      -6.0700     0.2000  1587.1503     5387.1220
Energy +pb_hcp_3.55/  2 -pb_hcp_2.82/  2   -63.0354     -83.2100     2.0000   101.7538     5488.8758
Energy +pb_hcp_3.55/  2 -pb_hcp_2.99/  2   -29.4887     -39.2300     1.0000    94.8929     5583.7686
Energy +pb_hcp_3.55/  2 -pb_hcp_3.15/  2   -12.5663     -16.8600     1.0000    18.4363     5602.2049
Energy +pb_hcp_3.55/  2 -pb_hcp_3.30/  2    -3.9952      -6.0900     1.0000     4.3884     5606.5933
Energy +pb_hcp_3.55/  2 -pb_hcp_3.43/  2    -1.5684      -1.6500     1.0000     0.0067     5606.6000
Energy +pb_hcp_3.55/  2 -pb_hcp_3.66/  2     0.6358      -0.2200     1.0000     0.7325     5607.3324
Energy +pb_hcp_3.55/  2 -pb_hcp_3.77/  2     0.8908      -1.5000     1.0000     5.7161     5613.0485
Energy +pb_hcp_3.55/  2 -pb_hcp_3.87/  2     0.9285      -3.2000     1.0000    17.0449     5630.0934
Energy +pb_hcp_3.55/  2 -pb_hcp_3.97/  2     0.8662      -5.0300     0.4000   217.2808     5847.3742
Energy +pb_hcp_3.55/  2 -pb_hcp_4.06/  2     0.7651      -7.2300     0.2000  1598.0287     7445.4028
```

Figure 7: A fort.99 file using lead crystals FCC, BCC, SC, and HCP. fort.99 is the file reporting the error in the force field. The first column is the column stating what type of parameter ReaxFF is comparing, only energy (kcal/mol) in this case. The next columns are energy comparisons between different crystal structures, divided by the number of atoms in the basis to get the energy per atom, instead of energy per unit cell. The next two columns, 'FField value' and 'QM/Lit value', are respectively the force field value and the data set value (found from the trainset.in file) of the energies of the crystal structures described in the foregoing columns. The 'Weight' column is the weighting (importance) of each row, also taken from the trainset.in file. The 'Error' column is calculated as shown in eq. 40. The 'Total error' column is summing up the parts in the 'Error' column.

20

2.2.5 params

In the params file one decides which ffield constants to vary for an optimization of the force field, the minimum and maximum value to vary between, and what step-size to use.

2.2.6 fort.4

After a force field optimization, the new force field constants are written into this file. The format of this file is exactly the same as the format for the ffield file, and can be used for a new force field optimization.

2.2.7 Optimizing a force field

The recipe for making/optimizing a force field, only taking the energy in the data set into consideration, is as follows:

1. Make a ffield file by inserting start values for all the constants that are to be included in the force field.

2. Make a params file and decide which of these constants ReaxFF should vary, and decide the minimum value, maximum value and step size for the process.

3. Make a trainset.in file. This file contains all the energies in the data set, and the weighting of each such energy.

4. Make a geo file. This file contains the geometries for the energies used in trainset.in.

5. Run a force field optimization job. The program will then vary each of the ffield constants as specified in the params file, one constant at a time, from the minimum to the maximum value. The value for the constant that makes the total error as small as possible, shown in the fort.99 file, is then chosen. This is done for all the constants refered to in the params file. The force field energy for the comparison is calculated by using the constants in the ffield file and the parameters in the geo file.

6. The new force field constants are displayed in the fort.4 file, so one should overwrite the ffield file with the fort.4 file.

7. Change some of the parameters in the trainset.in file and the params file if necessary.

8. The weighting in the trainset.in file, parameters in the params file, and constants in the ffield file can be varied. Go to point 5, and run the job until the results are satisfactory.

2.3 Density Functional Theory (DFT)

Density functional theory is an energy minimization method, using quantum mechanics. The main idea is to have the atom cores in fixed positions, and state that the electrons around the cores can be described as an electron density. The energy minimum is found by finding the corresponding electron density. The time-independend Schrödinger equation states that

$$\hat{H}\Psi = E\Psi \tag{41}$$

where E is the total energy of the system, Ψ is the wavefunction of the system and $\hat{H}$ is the Hamiltonian (the total energy operator). For a molecular system with no external field, excluding core-core repulsion, and approximating the nuclei to be point-charges at rest, the Hamiltonian is

$$\hat{H} = \hat{V}_{ext} + \hat{K} + \hat{V}_{ee} = -\sum_{i=1}^{N}\sum_{A=1}^{M} \frac{Z_A}{|\vec{R}_A - \vec{r}_i|} - \frac{1}{2}\sum_{i=1}^{N}\nabla_i^2 + \sum_{j=1}^{N}\sum_{i=1}^{j-1}\frac{1}{r_{ij}} \tag{42}$$

Here, $\hat{V}_{ext}$ is the attractive Coulomb operator due to the core potential, $\hat{K}$ is the kinetic energy operator for each separate electron, and $\hat{V}_{ee}$ is the electron-electron repulsion operator. N is the number of electrons in the system, M the number of nuclei, Z_A the number of protons for the different nuclei, r_{ij} the distance between electron i and j, and $|\vec{R}_A - \vec{r}_i|$ is the distance between the different nuclei and electrons.

2.3.1 Variational principle

For systems with two or more electrons, it is impossible to find the solution analytically. This is because of the electron-electron repulsion term $\hat{V}_{ee}$. Therefore it is necessary to use the variational principle, which states

$$E \leq \langle \Psi^t | \hat{H} | \Psi^t \rangle \tag{43}$$

that means for any trial wavefunction Ψ^t used in a system, the energy E of the ground state wavefunction will always be lower. This is because the ground state is defined as the state where the wavefunction will give the lowest possible energy. Therefore the challenge is to find a basis set of functions so that the total wavefunction Ψ^t gives an energy close enough to the real value to be satisfactory. There are two requirements

for the trial function Ψ^t. The first one, Ψ^t has to be square integrable and the square integral over all space, $\int \Psi^{t\dagger}\Psi^t d^3 r$, have to give the number of electrons in the system, N, as Ψ^t has to be normalized. The second requirement is the antisymmetry requirement, i.e, if any two electrons change wavefunctions the total wavefunction will change sign. Because the Shrödinger equation does not exclude the trial functions that do not meet the second requirement, the wavefunction to should be antisymmetric.

2.3.2 The first Hohenberg-Kohn Theroem

To prove that it is possible to define the whole system by using the electron density instead of the potential (that means the potential can be determined by only looking at the electron density), Hohenberg and Kohn have developed a theorem [14, 15]: Take two different external potentials $\hat{V}_{ext1}$ and $\hat{V}_{ext2}$ that differ by more than a constant. They will of course have different electron wavefunctions Ψ_1 and Ψ_2 as gound states. Then let us say the electrons in the two potentials have the same density. Then use Ψ_2 as a trial wavefunction for the potential $\hat{V}_{ext1}$. Then, by the variational principle (43) using the hamiltonian (42) we get

$$\langle \Psi_1 | \hat{V}_{ext1} + \hat{K} + \hat{V}_{ee} | \Psi_1 \rangle \leq \langle \Psi_2 | \hat{V}_{ext1} + \hat{K} + \hat{V}_{ee} | \Psi_2 \rangle \tag{44}$$

Because

$$\langle \Psi_1 | \hat{V}_{ext1} | \Psi_1 \rangle = \langle \Psi_1 | \Psi_1 \rangle \hat{V}_{ext1} \tag{45}$$

and

$$\langle \Psi_2 | \hat{V}_{ext1} | \Psi_2 \rangle = \langle \Psi_2 | \Psi_2 \rangle \hat{V}_{ext1} = \langle \Psi_1 | \Psi_1 \rangle \hat{V}_{ext1} \tag{46}$$

(the densities are supposed to be equal), (44) becomes

$$\langle \Psi_1 | \hat{K} + \hat{V}_{ee} | \Psi_1 \rangle \leq \langle \Psi_2 | \hat{K} + \hat{V}_{ee} | \Psi_2 \rangle \tag{47}$$

The kinetic energy operator and electron-electron interaction operator are the same in both expressions. If you use Ψ_2 as the ground state and Ψ_1 as the trialfunction, you get the same expression where just the wavefunctions are interchanged. This creates a contradiction unless the wavefunctions are the same, by the assumption of no degeneracy of the ground state. That means there is only one density allowed for any potential, which makes it possible to define the potential from the density, making it further possible to define the whole system by the density.

2.3.3 The second Hohenberg-Kohn Theorem

The second Hohenberg-Kohn theorem proves that the variational principle holds for an electron density as well as an electron wavefunction, i.e,

$$E(\rho(r)) \leq E(\rho'(r)) \tag{48}$$

23

Here, ρ determines $\hat{V}_{ext}$, $\hat{V}_{ext}$ determines $\hat{H}$, and $\hat{H}$ determines Ψ. Therefore, Ψ is a functional of $\rho(r)$, and so the expectation value of $\hat{H}$ is

$$E(\rho(r)) = \langle \Psi | \hat{H} | \Psi \rangle \tag{49}$$

Here, $E(\rho(r))$ is the ground state energy and $E(\rho'(r))$ is the energy caused by the electron density $\rho'(r)$. Ψ is the wavefunction corresponding to the ground state electron density $\rho(r)$, and Ψ' is the wavefunction corresponding to the electron density $\rho'(r)$.

$$E(\rho'(r)) = \langle \Psi' | \hat{H} | \Psi' \rangle \tag{50}$$

Inserting (49) and (50) into (43) for these two densities, it is found

$$\langle \Psi | \hat{H} | \Psi \rangle \leq \langle \Psi' | \hat{H} | \Psi' \rangle \tag{51}$$

and therefore

$$E(\rho(r)) \leq E(\rho'(r)) \tag{52}$$

2.3.4 The Kohn-Sham procedure

The density of electrons can be defined as [16]

$$\rho(r) = \sum_{i=1}^{N} |\psi_i(r)|^2 \tag{53}$$

where $\psi_i(r)$ are wavefunctions. Using the electron density, $\rho(r)$, we can write the total energy obtained from the Schrödinger equation as

$$E = \langle \Psi | \hat{H} | \Psi \rangle = \int \hat{V}_{ext}(r)\rho(r)dr + \langle \Psi | \hat{K} + \hat{V}_{ee} | \Psi \rangle \tag{54}$$

Now, consider the hamiltonian

$$\hat{H} = \hat{V}_{ext\lambda} + \hat{K} + \lambda\hat{V}_{ee} \tag{55}$$

where λ can vary between 0 and 1. Here, $\hat{V}_{ext\lambda}$ is a potential that varies with λ such that the electron density ρ always is that of the real system. Then, for $\lambda = 1$, the hamiltonian is equal to the energy operator of the real system (42). $\lambda = 0$ corresponds to a system without the electron-electron interaction term $\hat{V}_{ee}$, with the density of the real system in the potential $\hat{V}_{ext1}$. The Hellmann-Feynman theorem [17] states

$$\frac{dE}{d\lambda} = \frac{\langle \Psi | \partial\hat{H}/\partial\lambda | \Psi \rangle}{\Psi\Psi} \tag{56}$$

24

When integrating (56) from $\lambda = 0$ to $\lambda = 1$, the result is

$$E(\lambda = 1) - E(\lambda = 0) = \int_0^1 \frac{\langle \Psi | \partial \hat{H} / \partial \lambda | \Psi \rangle}{\Psi \Psi} d\lambda \tag{57}$$

Calculating the derivative $\partial \hat{H} / \partial \lambda$ one obtains

$$\frac{\partial \hat{H}}{\partial \lambda} = \frac{\partial (\hat{K} + \hat{V}_{ext\lambda} + \lambda \hat{V}_{ee})}{\partial \lambda} = \frac{\partial \hat{V}_{ext\lambda}}{\partial \lambda} + \hat{V}_{ee} \tag{58}$$

Putting (58) into (56), and moving $E(\lambda = 0)$ over to the right side of the equation, and writing out for $E(\lambda = 0)$, one obtains

$$E(\lambda = 1) = K_{ni} + V_{ext0} + \int_0^1 \langle \Psi | \hat{V}_{ee} | \Psi \rangle d\lambda + \int_0^1 \frac{\langle \Psi | \partial V_{ext\lambda} / \partial \lambda | \Psi \rangle}{\Psi \Psi} d\lambda \tag{59}$$

$$= K_{ni} + V_{ext0} + \int_0^1 \langle \Psi | \hat{V}_{ee} | \Psi \rangle d\lambda + V_{ext1} - V_{ext0} = K_{ni} + V_{ext1} + \int_0^1 \langle \Psi | \hat{V}_{ee} | \Psi \rangle d\lambda \tag{60}$$

The electron density is the same for the interacting and the non-interacting system, K_{ni} and V_{ext1} are easily found, just using the kinetic energy operator and potential operator on the Slater-determinant [18] of the non-interacting density. The integral over the electron-electron interaction $\int_0^1 \langle \Psi | \hat{V}_{ee} | \Psi \rangle d\lambda$ still remains unsolved. Splitting the integral into a classical Coloumb interaction part and an exchange-correlation part makes it more convenient for later on. The exchange and the correlation energies are the final unknown pieces of energy. Correlation energy is an energy term used for correcting the total energy. It is needed for correcting for the equation found in [19] that is an equation obtained using first order perturbation theory:

$$E_k = \int \Psi_k \Delta v(r_1) \Psi_k d^3 r \tag{61}$$

where Δv is the perturbation. The equation is used for finding (56). The correlation energy also corrects for approximations made later on. Writing out for the integral

$$\int_0^1 \langle \Psi | \hat{V}_{ee} | \Psi \rangle d\lambda = \frac{1}{2} \int \int dr_1 dr_2 \frac{\rho(r_1) \rho(r_2)}{|r_1 - r_2|} + E_{XC}(\rho) \tag{62}$$

The total energy is then shown:

$$E(\rho) = K_{ni}(\rho) + V_{ext1}(\rho) + V_{classee}(\rho) + E_{XC}(\rho) \tag{63}$$

The only energy term that is not determined is $E_{XC}(\rho)$, the exchange and correlation energy. The exchange energy is the electron-electron interaction of the non-diagonal elements in the Slater determinant.

2.3.5 Local Density Approximation

The first expression made for finding E_{XC} was the *local density approximation*, LDA. Here you ignore all other electron densities than the one you look at right now, i.e you do not look at electron densities close by to determine the density gradient. The ideal electron gas requires a uniform positive charge of equal density to be stationary. This causes the potentials in (63) to cancel out, and the LDA energy becomes

$$E(\rho)^{LDA} = K_{ni}^{LDA}(\rho) + E_{XC}^{LDA}(\rho) \tag{64}$$

For an infinitely deep cubic well the energy levels (only kinetic energy) for a particle are given as [20]

$$\epsilon = \frac{h^2}{8ml^2}(n_x^2 + n_y^2 + n_z^2) = \frac{h^2}{8ml^2}R^2 \tag{65}$$

Here, l is the lenght of the sides of the cube, m is the electron mass, h is Planck's constant and n_x, n_y, and n_z are the excitation numbers in the different directions. The number of energy levels Φ with less energy than ϵ can then be written as one octant of a sphere with radius R.

$$\Phi(\epsilon) = \frac{1}{8}\frac{4\pi R^3}{3} = \frac{\pi}{6}\left(\frac{8ml^2\epsilon}{h^2}\right)^{3/2} \tag{66}$$

The number of energy levels between ϵ and $\epsilon + d\epsilon$ is then (differentiating (66))

$$g(\epsilon)d\epsilon = \Phi(\epsilon + d\epsilon) - \Phi(\epsilon) = \frac{\pi}{4}\left(\frac{8ml^2}{h^2}\right)^{3/2}\epsilon^{1/2}d\epsilon \tag{67}$$

At zero temperature the Fermi energy ϵ_F is the upper energy limit of occupied states, and all states below this energy are occupied (no excited states at 0K.) The total energy of all the electrons in this well is

$$K_{ni}^{LDA} = 2\int_0^{\epsilon_F} \epsilon g(\epsilon)d\epsilon = 4\pi\left(\frac{2m}{h^2}\right)^{3/2}l^3\int_0^{\epsilon_F}\epsilon^{3/2}d\epsilon = \frac{8\pi}{5}\left(\frac{2m}{h^2}\right)^{3/2}l^3\epsilon_F^{5/2} \tag{68}$$

where the factor 2 comes from the Pauli principle. The number of electrons in the well as a function of the Fermi energy is

$$N = 2\int_0^{\epsilon_F} g(\epsilon)d\epsilon = \frac{8\pi}{3}\left(\frac{2m}{h^2}\right)^{3/2}\epsilon_F^{3/2} \tag{69}$$

Eliminating ϵ_F by combining (68) and (69) gives

$$K_{ni}^{LDA} = \frac{3h^2}{10m}\left(\frac{3}{8\pi}\right)^{2/3}l^3\left(\frac{N}{l^3}\right)^{5/3} = \frac{3h^2}{10m}\left(\frac{3}{8\pi}\right)^{2/3}l^3\rho^{5/3} \tag{70}$$

Here, ρ is the electron density, the number of electrons N divided by the volume l^3. To include electron-electron interaction in the system, exchange and correlation energy is also required. The total exchange energy E_X^{LDA} between electrons in spin-orbitals χ_i and χ_j is [21]

$$E_X^{LDA} = \sum_{i=1}^{N} \sum_{j=i+1}^{N} \int \int d^3r_1 d^3r_2 \chi_i(1)\chi_j(2) \left(\frac{1}{r_{12}}\right) \chi_i(2)\chi_j(1) \tag{71}$$

Evaluating this equation using the Slater determinant for plane waves in an infinitely deep well, you get

$$\begin{aligned} E_X^{LDA} &= -\int d^3r \frac{3}{4} \left(\frac{3}{\pi}\rho\right)^{1/3} \rho \\ &= -\frac{3}{4} \left(\frac{3}{\pi}\right)^{1/3} \int d^3r \rho^{4/3} \end{aligned} \tag{72}$$

The correlation energy is much more complicated, as it depends on the physical ground state, and not on the non-interacting ground state. We will therefore not go much into detail here. By studying the limits of the density, $\rho \to \infty$ and $\rho \to 0$, one finds the energy using perturbation theory. The two expressions found for each limit can be extrapolated for the section between the two limits of ρ. The total expression is found to be [22]

$$\begin{aligned} E_C^{LDA} &= 1.105r_s^{-2} - 0.458r_s^{-1} + 0.0311\ln r_s \\ &\quad - 0.048 - 0.018r_s + 0.009r_s \ln r_s + O(r_s^2 \ln r_s) \end{aligned} \tag{73}$$

where $r_s = (4\pi\rho/3)^{-1/3}$, and r_s is the radius of a sphere with volume equal to V/N where V is the volume and N is the number of electrons in a uniform electron gas. In Ref. [22] units of Rydberg instead of Hartree were used, so all numbers here are divided by two in comparison to the original formula. For r_s between 2 and 5, (73) will not give an accurate account, i.e, the error is larger than $5 \cdot 10^{-3}$ due to extrapolation errors.

2.3.6 Generalized Gradient Approximation (GGA)

Some researchers have seen the need for improvement of the energy predicted by LDA. This is because not all the kinetic energy is included in the LDA, giving energies calculated with LDA a lower energy than the real system. This is because GGAs are a function of the gradient of the density ($\nabla\rho$) as well as the density (ρ). GGAs then favor density inhomogenety more than LDA, as commented in Ref. [23]. Here is

described three of the GGAs available in the ADF package. The global Lieb-Oxford bound [24] states the maximum underestimation error LDA can make for the exchange and correlation energy, and all GGA exchange energy functionals can be written as

$$E_X = \int d^3 r \epsilon_X^{LDA} F(\rho, \nabla \rho) \tag{74}$$

If the exchange enhancement factor $F(\rho, \nabla \rho)$ exceeds the Lieb-Oxford bound, it will always overestimate the energy correction. None of the functionals below are in conflict with the global Lieb-Oxford bound. The *local* Lieb-Oxford bound states the maximum limit of the GGA exchange and correlation energy *density*, $\epsilon_X^{LDA} \cdot F(\rho, \nabla \rho)$. The energy densities ϵ_C^{LDA} and ϵ_X^{LDA} are the local values of the correlation and exchange energy density, respectively.

PW91 Perdew-Wang exchange and correlation functional PW91 is designed to be a first-principles numerical GGA and to be fitting several conditions as commented in Ref. [25]. The functional has a scary number of terms [26, 27, 28]

$$E_X^{PW91} = E_X^{LDA} \left(\frac{1 + s a_1 \sinh^{-1}(s a_2) + (a_3 + a_4 e^{-100 s^2}) s^2}{1 + s a_1 \sinh^{-1}} + a_5 s^4 \right) \tag{75}$$

$$s = \frac{|\nabla \rho|}{(24 \pi^2)^{1/3} \rho^{4/3}} \tag{76}$$

Here, $a_1 = 0.19645$, $a_2 = 7.7956$, $a_3 = 0.2743$, $a_4 = $ -0.1508, and $a_5 = 0.004$. The correlation energy is

$$E_C^{PW91} = E_C^{LDA} + \rho \frac{\beta^2}{2\alpha} \ln \left(1 + \frac{2\alpha}{\beta} \frac{t^2 + A t^4}{1 + A t^2 + A^2 t^4} \right) + C_{c0}(C_c(\rho) - C_{c1}) t^2 e^{-100 s^2} \tag{77}$$

$$A = \frac{2\alpha}{\beta} \left(e^{-2\alpha \, E_C^{LDA}/(\rho \beta^2)} - 1 \right)^{-1} \tag{78}$$

$$t = \frac{(\pi/3)^{1/6}}{4} \frac{|\nabla \rho|}{\rho^{7/6}} \tag{79}$$

$\alpha = 0.09$, $\beta = 0.0667263212$, $C_{c0} = 15.7559$, $C_{c1} = 0.0035521$

$$C_c(\rho) = C_1 + \frac{C_2 + C_3 r_s + C_4 r_s^2}{1 + C_5 r_s + C_6 r_s^2 + C_7 r_s^3}. \tag{80}$$

$C_1 = 0.001667$, $C_2 = 0.002568$, $C_3 = 0.023266$, $C_4 = 7.389 \cdot 10^{-6}$, $C_5 = 8.723$, $C_6 = 0.472$, $C_7 = 0.07389$. As in 2.3.5, $r_s = (4\pi \rho/3) - 1/3$.

28

BLYP The Becke exchange functional is implemented to give the correct $1/r$ behavior of the exchange energy density for $r \to \infty$ [29]. This criterion is not statisfied in PW91. The Becke88 exchange energy is given as [29]

$$E_X^{B88} = E_X^{LDA} - \beta \sum_\sigma \int \rho_\sigma^{4/3} \frac{x^2}{1 + 6\beta x \sinh^{-1} x} d^3r \tag{81}$$

where σ denotes either "up" or "down" spin.

$$x = \frac{|\nabla \rho_\sigma|}{\rho_\sigma^{4/3}} \tag{82}$$

Becke obtained the constant $\beta = 0.0042$ by fitting to Hartree-Fock calculations of the noble gas atoms. The LYP (Lee, Yang, Parr) correlation functional is [30]

$$E_C^{LYP} = -a \frac{1}{1 + d\rho^{-1/3}} \left(\rho + b\rho^{-2/3}(C_F \rho^{5/3} - 2t_W + \frac{1}{9}(t_W + \frac{1}{2}\nabla^2 \rho))e^{-c\rho^{-1/3}} \right) \tag{83}$$

$$t_W = \frac{1}{8} \left(\frac{|\nabla \rho|^2}{\rho} - \nabla^2 \rho \right) \tag{84}$$

with $C_F = \frac{3}{10}(3\pi^2)^{2/3}$, $a = 0.04918$, $b = 0.132$, $c = 0.2533$, and $d = 0.349$. The LYP functional is the density-functional form of the Colle-Salvetti formula [31] that gives an approximate calculation for the correlation energy in the form of the density and a Laplacian of the second-order density matrix used in Hartree-Fock theory. The LYP functional has been tested against the Colle-Salvetti formulas and found to have about the same accuracy [30], about a few percent off.

RPBE The PBE (Perdew Burke Ernzerhof) exchange and correlation GGA functional only contains components that are fundamental constants [32] (except the LDA ones). The functional is meant to be a simplification of PW91 by removing less energetically significant conditions. These are:

- Correct second-order gradient coefficient for slowly varying limits.

- Correct uniform scaling of E_X where $s \to \infty$ (s is the reduced gradient that has already appeared in PW91).

In addition to simplifying the functional, there are some problems in PW91 that PBE fixes. These are described in Ref. [32]. The PBE exchange and correlation functionals are [32]

$$E_X^{PBE} = \int d^3r \rho e_x^{unif} F_X(s) \tag{85}$$

$$F_X(s) = 1 + \kappa - \frac{\kappa}{1 + \mu s^2/\kappa} \tag{86}$$

$\kappa = 0.804$, $\mu = \beta(\pi^2/3)$ and β is the same as for PW91, 0.066725. s is the reduced density gradient (here the density is denoted as n.)

$$s(r) = \frac{|\nabla n|}{2k_F n} \tag{87}$$

where k_F is the Fermi wave-vector.

$$E_C^{PBE} = \int d^3 r n \cdot \left(\epsilon_C^{LDA} + F_C \right) \tag{88}$$

$$F_C = \frac{e^2}{a_0} \gamma \phi^3 \ln \left(1 + \frac{\beta}{\gamma} t^2 \left(\frac{1 + At^2}{1 + At^2 + A^2 t^4} \right) \right) \tag{89}$$

where

$$A = \frac{\beta}{\gamma} \left(\exp \left[-\epsilon_C^{LDA} / \left(\gamma \phi^3 e^2/a_0 \right) \right] - 1 \right)^{-1} \tag{90}$$

Here, $e =$ the electron charge, $a_0 =$ the Bohr radius, $\gamma = (1 - \ln 2)/\pi^2$, $t = |\nabla n|/(2\phi\sqrt{4k_F/(\pi a_0)}n$, $\phi = ((1 + \xi)^{2/3} + (1 - \xi)^{2/3})/2$. ξ is the relative spin polarization, $(n_\uparrow - n_\downarrow)/n$. RPBE [33] is a modification of PBE, using another exchange enhancement factor F_X, changing it from (86) to

$$F_X(s) = 1 + \kappa \left(1 - e^{-\mu s^2/\kappa} \right) \tag{91}$$

κ is still 0.804. This form gives better values for medium and high s values and satisfies the local Lieb-Oxford bound [33].

2.3.7   Zeroth-Order Regular Approximation (ZORA)

ZORA is a method for correcting the hamiltonian for relativistic energy and spin-orbit coupling. Without such corrections, the kinetic energy operator $\hat{K}$ is

$$\hat{K} = \frac{1}{2}\vec{p} \cdot \vec{p} \tag{92}$$

where $\vec{p}$ is the momentum operator, ∇/i.

ZORA Scalar Relativistic   The total energy for scalar (not quantum mechanical) relativistic energy W_{SR} is

$$W_{SR} = (c^4 + p^2c^2)^{1/2} + V \tag{93}$$

Using atomic units, the electron mass, m, has been set to 1. Disregarding the rest-mass energy, the energy is

$$E_{SR} = W_{SR} - c^2 \tag{94}$$

Substituting for W_{SR} by inserting (93) in (94) gives

$$E_{SR} = (c^4 + p^2c^2)^{1/2} - c^2 + V \tag{95}$$

which may be rewritten as, by multiplying with and dividing by $c^2 + (c^4 + p^2c^2)^{1/2}$,

$$E_{SR} = \frac{p^2c^2}{c^2 + (c^4 + p^2c^2)^{1/2}} + V \tag{96}$$

By substituting $(c^4 + p^2c^2)^{1/2} - c^2$ with $E_{SR} - V$ from (95), (96) can be rewritten to

$$E_{SR} = \frac{p^2c^2}{2c^2 + E_{SR} - V} + V \tag{97}$$

Because $2c^2 - V$ is much larger than E_{SR}, (97) can be approximated to, or expanded in the zeroth order to

$$E_{SR} \approx \frac{p^2c^2}{2c^2 - V} + V = K_{SR}^{ZORA} + V \tag{98}$$

For the kinetic energy, $(p^2c^2)/(2c^2 - V)$, the behavior is good also for $r \to 0$ where $V \to \infty$. The scalar relativistic energy matrix element is

$$E_{SR,ab}^{ZORA} = \langle \psi_a | V + \vec{p} \frac{c^2}{2c^2 - V} \vec{p} | \psi_b \rangle \tag{99}$$

ZORA spin-orbit   The quantum mechanical relativistic energy operator is given by the Dirac equation as [34]

$$\hat{H}'_{SO} = (c^4 + c^2\vec{p}^2)^{1/2} = c\vec{\alpha} \cdot \vec{p} + \beta c^2 \tag{100}$$

Adding a potential operator $\hat{V}$ and substracting for the electron rest mass energy gives an energy operator suitable for DFT:

$$\hat{H}_{SO} = (c^4 + \vec{p}^2c^2)^{1/2} + \hat{V} - c^2 = c\vec{\alpha} \cdot \vec{p} + \beta c^2 + \hat{V} - c^2 \tag{101}$$

31

Here, α and β are given in Ref. [35] as

$$\vec{\alpha}_k = \begin{pmatrix} 0 & \vec{\sigma}_k \\ \vec{\sigma}_k & 0 \end{pmatrix}, \quad \beta = \begin{pmatrix} 1 & 0 \\ 0 & -1 \end{pmatrix} \tag{102}$$

Here, $k = 1, 2, 3$, and 1, 0, and $\vec{\sigma}_k$ represent 2×2 matrices, and $\vec{\sigma}_k$ are the Pauli matrices:

$$\vec{\sigma}_1 = \begin{pmatrix} 0 & 1 \\ 1 & 0 \end{pmatrix}, \quad \vec{\sigma}_2 = \begin{pmatrix} 0 & -i \\ i & 0 \end{pmatrix}, \quad \vec{\sigma}_3 = \begin{pmatrix} 1 & 0 \\ 0 & -1 \end{pmatrix} \tag{103}$$

and

$$0 = \begin{pmatrix} 0 & 0 \\ 0 & 0 \end{pmatrix}, \quad 1 = \begin{pmatrix} 1 & 0 \\ 0 & 1 \end{pmatrix} \tag{104}$$

Putting the 2×2 matrices for β and $\vec{\alpha}$ into (101), and using $\hat{H}_{SO}\Psi = E_{SO}\Psi$ gives two equations (Ψ has two components, ϕ and ξ, where ϕ and ξ are both two-component wavefunctions):

$$V\phi + c\vec{\sigma} \cdot \vec{p}\xi = E_{SO}\phi \tag{105}$$

and

$$c\vec{\sigma} \cdot \vec{p}\phi + (V - 2c^2)\xi \equiv E_{SO}\xi \tag{106}$$

Expressing ξ explicitly and eliminating ξ from (105) and (106) gives

$$\xi = \frac{1}{2c^2 + E_{SO} - V} c\vec{\sigma} \cdot \vec{p}\phi \equiv \hat{X}\phi \tag{107}$$

and

$$V\phi + \frac{1}{2}\vec{\sigma} \cdot \vec{p}\left(1 + \frac{E_{SO} - V}{2c^2}\right)^{-1}\phi \equiv \hat{H}_{SO}^1\phi = E_{SO}^1\phi \tag{108}$$

where Ψ is normalized, whereas ϕ is not. Further, $\Phi = O\phi$ where Φ is a twocomponent and normalized wavefunction and O is the normalization operator to be derived below. Writing out for the normalization of Ψ

$$\int \Phi^\dagger \Phi d^3r = \int \phi^\dagger O^\dagger O\phi d^3r = \int \Psi^\dagger \Psi d^3r$$
$$= \int (\phi^\dagger\xi + \xi^\dagger\phi + \phi^\dagger\phi + \xi^\dagger\xi)d^3r) = \int (\phi^\dagger\phi + \xi^\dagger\xi)d^3r = 1 \tag{109}$$

The cross-terms $\int \phi^\dagger\xi d^3r$ and $\int \xi^\dagger\phi d^3r$ vanish because the wavefunctions are orthogonal. Eliminating ξ when using (107) gives

$$1 = \int (\phi^\dagger\phi + \xi^\dagger\xi)d^3r = \int \phi^\dagger(1 + \hat{X}^\dagger\hat{X})\phi d^3r \tag{110}$$

32

One of the two solutions for O is then

$$O = (1 + \hat{X}^\dagger \hat{X})^{1/2} \tag{111}$$

The hamiltonian $\hat{H}_{SO}$ for Φ becomes

$$\hat{H}_{SO} = O\hat{H}^1_{SO}O^{-1} = (1 + \hat{X}^\dagger \hat{X})^{1/2}(V + c\vec{\sigma} \cdot \vec{p}\hat{X})(1 + \hat{X}^\dagger \hat{X})^{-1/2} \tag{112}$$

Expanding O to zeroth order (remember $\vec{\sigma}^2 = 1$), and eliminating $(E_{SO} - V)/(2c^2) \ll 1$ in O gives

$$O \approx (1 + p^2/4c^2 + ...) \approx 1 \tag{113}$$

Writing out for $\hat{H}^{ZORA}_{SO}$ gives

$$\hat{H}^{ZORA}_{SO} = V + c\vec{\sigma} \cdot \vec{p} \frac{1}{2c^2 + E^{ZORA}_{SO} - V}\vec{\sigma} \cdot \vec{p} \tag{114}$$

Because $2c^2 - V$ is much larger than E^{ZORA}_{SO}, $\hat{H}^{ZORA}_{SO}$ can be approximated to, or expanded in the zeroth order to

$$\hat{H}^{ZORA}_{SO} = V + c\vec{\sigma} \cdot \vec{p} \frac{1}{2c^2 - V}\vec{\sigma} \cdot \vec{p} = \hat{K}^{ZORA}_{SO} + V \tag{115}$$

The energy matrix element $E^{ZORA}_{SO,ab}$ is then

$$E^{ZORA}_{SO,ab} = \langle \psi_a | V + \vec{\sigma} \cdot \vec{p} \frac{c^2}{2c^2 - V}\vec{\sigma} \cdot \vec{p} | \psi_b \rangle \tag{116}$$

2.3.8 Basis sets

Now we finally have the energy operator ready. The next step is to decide on a basis set that can give a good physical description of the system. We will here only look at basis sets that include linear combinations of wavefunctions ϕ_a.

$$\psi_i = \sum_a^K c_{ai}\phi_a \tag{117}$$

Here, ϕ_a is one of the basis functions constructing the electron orbital i, ψ_i, and c_{ai} are the coefficients for each of these basis functions. For DFT, the basis sets of this form are *Slater orbitals*, *Gaussian functions* and *numerical basis functions*. The hydrogen atom wavefunctions are wavefunctions in a system with no electron-electron interaction, only interacting with one core Coulomb potential. The hydrogen atom orbitals are not particularly convenient even if the screening effect (the outermost

electrons are pushed outwards and the innermost are pushed closer to the nucleus) is accounted for. This is due to the complicated functional form of the hydrogen orbitals. The hydrogen orbitals have the form

$$\psi_{nlm} = R_{nl}(r)Y_{lm}(\theta, \phi) \tag{118}$$

Here θ and ϕ are angles. R is a radial function and Y is a spherical harmonic function.

Slater Type Orbitals (STOs)   To make a wavefunction easier to calculate, Slater (1930) [36] suggested a simpler analytical form for the radial functions, that only depends on the radial excitation, n.

$$R_n = (2\zeta)^{n+1/2}((2n)!)^{-1/2}r^{n-1}e^{-\zeta r} \tag{119}$$

Here, $(2\zeta)^{n+1/2}((2n))^{-1/2}$ is the normalization constant and n is an integer. ζ differs for different orbitals and atoms (the 2s orbital in oxygen is different from 2s orbital in lead,) and was found from experimental data (STOs today use better ζ values). Y is still the same as in hydrogen atom wavefunctions. It is not possible to integrate Slater type orbitals analytically.

Gaussian Type Orbitals (GTOs)   Gaussian type orbitals have been used frequently in the Hartree-Fock method, and it is no surprise it has been tested for DFT. For cartesian coordinates they have the form [37]

$$x^a y^b z^c \exp(-\alpha r^2) \tag{120}$$

and are normalized. Here, a, b, and c are positive integers or zero. The STOs are much closer to the real orbitals than GTOs. However, a linear combination of more Gaussians can give an imitation of a Slater orbital. You need at least 3 such orbitals to get any reasonable results. The reason to use Gaussians is that the product of two Gaussian functions (centered at different atoms) is just another Gaussian function. Because of this, they can be integrated analytically and therefore takes less CPU time.

Numerical basis functions   Numerical basis functions can be generated by solving the Kohn-Sham equations for isolated atoms. Solving the integrals numerically, you get a set of values for the density in a polar grid centered on each atom. Then you calculate the density gradient around all atoms.

Use of spin in basis functions For systems with closed outermost shells, all electrons are paired, with spin up or down. This property is used to greatly reduce the size of closed shell systems as the orbitals are the same for two and two electrons. For an open shell (i.e the outermost shell is not filled up) the electrons in the outermost shell often have the same spin as this will push them away from each other to lower the energy. The pairing of electrons will in this case give a wavefunction that is not the ground state.

2.3.9 The DFT version of the Roothaan-Hall equations

The Shrödinger equation is

$$\hat{H}\Psi = E\Psi \tag{121}$$

where $\hat{H}$ is the energy operator and E is the energy. The Shrödinger equation for molecular orbital ψ_i (interacting with all other orbitals) looks like

$$\hat{H}\psi_i = \epsilon_i \psi_i \tag{122}$$

$$\Rightarrow \hat{H} \sum_{a=1}^{F} c_{ia}\phi_a = \epsilon_i \sum_{a=1}^{F} c_{ia}\phi_a \tag{123}$$

Here we used (117) to substitute ψ_i. Multiplying each side by ϕ_b and integrating each side gives

$$\sum_{a=1}^{F} c_{ia} \int d^3r \phi_b \hat{H}\phi_a = \epsilon_i \sum_{a=1}^{F} c_{ia} \int d^3r \phi_b \phi_a \tag{124}$$

On matrix form (124) becomes

$$\mathbf{HC} = \mathbf{SCE} \tag{125}$$

where $c_{a,b}$ are the basis function coefficients

$$\mathbf{C} = \begin{pmatrix} c_{1,1} & c_{1,2} & ... & c_{1,D} \\ c_{2,1} & c_{2,2} & ... & c_{2,D} \\ ... & ... & ... & ... \\ c_{D,1} & c_{D,2} & ... & c_{D,D} \end{pmatrix} \tag{126}$$

and ϵ_a are the energies for each orbital

$$\mathbf{E} = \begin{pmatrix} \epsilon_1 & 0 & ... & 0 \\ 0 & \epsilon_2 & ... & 0 \\ ... & ... & ... & ... \\ 0 & 0 & ... & \epsilon_D \end{pmatrix} \tag{127}$$

and **H** is the energy contribution for all orbital combinations.

$$\mathbf{H} = \begin{pmatrix} H_{1,1} & H_{1,2} & ... & H_{1,D} \\ H_{2,1} & H_{2,2} & ... & H_{2,D} \\ ... & ... & ... & ... \\ H_{D,1} & H_{D,2} & ... & H_{D,D} \end{pmatrix} \tag{128}$$

Here, $H_{a,b}$ is the energy produced by the density $\langle \phi_a | \phi_b \rangle$. When not using ZORA $H_{a,b}$ is given by equation (63)

$$\int d^3r_1 \phi_b \hat{H} \phi_a = H_{a,b} = \int d^3r_1 \phi_b(r_1) \left(-\frac{\nabla^2}{2} - \sum_{A=1}^{M} \frac{Z_A}{r_{1A}} \right) \phi_a(r_1)$$

$$+ \int d^3r \frac{\partial E_{XC}(r_1)}{\partial \rho(r_1)} + \int \int d^3r_1 d^3r_2 \phi_b(r_1) \frac{\rho(r_2)}{r_{12}} \phi_a(r_1) \tag{129}$$

The overlap matrix that decides how much two orbitals overlap each other,

$$\mathbf{S} = \begin{pmatrix} \int d^3r \phi_1 \phi_1 & \int d^3r \phi_1 \phi_2 & ... & \int d^3r \phi_1 \phi_D \\ \int d^3r \phi_2 \phi_1 & \int d^3r \phi_2 \phi_2 & ... & \int d^3r \phi_2 \phi_D \\ ... & ... & ... & ... \\ \int d^3r \phi_D \phi_1 & \int d^3r \phi_D \phi_2 & ... & \int d^3r \phi_D \phi_D \end{pmatrix} \tag{130}$$

All the elements in $H_{a,b}$ have low CPU cost except the Coloumb interaction part

$$\int \int d^3r_1 d^3r_2 \frac{\rho(r_2)\phi_a \phi_b}{r_{12}} \tag{131}$$

Poisson's equation states that

$$V_{el}(r_1) = \int \frac{\rho(r_2)}{|r_1 - r_2|} d^3r_2 \tag{132}$$

A well-known derivation from Maxwell equations states the differential Poisson's equation

$$\nabla^2 V(r_1) = -4\pi\rho(r_1) \tag{133}$$

and so, combining (132) and (133) gives

$$\nabla^2 \int \frac{\rho(r_2)}{|r_1 - r_2|} d^3r_2 = -4\pi\rho(r_1) \tag{134}$$

To find $V_{el}(r_1)$, eq. (134) can be solved numerically on a grid. Then $V_{el}(r_1)$ can be inserted into (131) giving

$$\int \int d^3r_1 d^3r_2 \frac{\rho(r_2)\phi_a \phi_b}{r_{12}} = \int d^3r_1 \phi_a(r_1) V_{el}(r_1) \phi_b(r_1) \tag{135}$$

This integral is then solved numerically using the same grid used for finding $V_{el}(r_1)$. To find the coefficients $c_{a,b}$, you need to have a matrix of the form $\mathbf{FC} = \mathbf{CE}$. This is done by finding a matrix $\boldsymbol{\Xi}$ that has the ability $\boldsymbol{\Xi}^{\mathbf{T}}\mathbf{S}\boldsymbol{\Xi} = \mathbf{I}$. How to do that will not be shown. From now on $\boldsymbol{\Xi}_{\mathbf{T}}$ is to be denoted as $\mathbf{S}^{-1/2}$. By multiplying (125) by $\mathbf{S}^{-1/2}$ on both sides of the equation, you get

$$\mathbf{S}^{-1/2}\mathbf{HC} = \mathbf{S}^{1/2}\mathbf{CE} \tag{136}$$

Inserting the identity matrix $\mathbf{I}$ in the form of $\mathbf{S}^{-1/2}\mathbf{S}^{1/2}$ between $\mathbf{H}$ and $\mathbf{C}$ on the left side gives

$$\mathbf{S}^{-1/2}\mathbf{HS}^{-1/2}\mathbf{S}^{1/2}\mathbf{C} = \mathbf{S}^{1/2}\mathbf{CE} \tag{137}$$

You can now express the matrix equation by $\mathbf{C}' = \mathbf{S}^{1/2}\mathbf{C}$, $\mathbf{H}' = \mathbf{S}^{-1/2}\mathbf{HS}^{-1/2}$, and $\mathbf{E}$:

$$\mathbf{H}'\mathbf{C}' = \mathbf{C}'\mathbf{E} \tag{138}$$

The eigenvalues of $\mathbf{E}$ can be found by solving the determinant $|\mathbf{H}'$ - $\mathbf{EI}| = 0$. Then, as the matrix of coefficients $\mathbf{C}'$ are the eigenvectors of $\mathbf{H}'$, you can find the coefficients in $\mathbf{C}'$ by diagonalising $\mathbf{H}$. Then it is easy to extract the coefficients of $\mathbf{C} = \mathbf{S}^{-1/2}\mathbf{C}'$. From $\mathbf{C}$ you can calculate a density ρ. The whole process goes as:

1. Calculate the integrals for kinetic energy, potential energy and the exchange correlation function to form the Energy matrix, $\mathbf{H}$.

2. Calculate the overlap matrix, $\mathbf{S}$

3. Form $\mathbf{S}^{-1/2}$

4. Guess or calculate an initial density, ρ, that is $\sum_{i=1}^{N} c_{ci}c_{di}\phi_c\phi_d$ for the N basis functions.

5. Form the $\mathbf{H}$ matrix using the integrals above and the density ρ

6. Form $\mathbf{H}' = \mathbf{S}^{-1/2}\mathbf{FS}^{-1/2}$

7. Find the eigenvalues of $\mathbf{E}$ from $|\mathbf{H}'$ - $\mathbf{EI}| = 0$. Find the $\mathbf{C}'$ coefficients by diagonalising $\mathbf{H}'$. Calculate the coefficients in $\mathbf{C}$ from $\mathbf{C}'$

8. Calculate ρ

9. Check the calculation for convergence (check if ρ is the same as before). If the calculation has not converged, go back to step 5.

The total energy is given by [38]

$$E = \sum_{i=1}^{N} \epsilon_i - V_{classee} + E_{XC} - \int \frac{\partial E_{XC}}{\partial \rho} \rho dr \qquad (139)$$

$\partial E_{XC}/\partial \rho$ is the functional derivative of the density. It is important to notice that this method is only for finding the minimum energy given nuclei locked in position. To find the minimum for systems where the nuclei can be moved, one has to use some method for finding the coordinate derivative for the cores in respect to the energy, and also include the core-core repulsion energy that is normal Coloumb repulsion.

2.4 Approximations

An approximation always used, except for when dealing with small systems, is an approximation that neglects some overlaps (what we choose to call *zero overlap approximation*), as the overlap of basis functions centered far from each other are very small. When many of the terms in the overlap matrix are zero, fewer integrals need to be calculated. The *frozen core approximation* freezes the orbitals of the electrons closest to the core when atoms are brought together to make molecules. Although the change in kinetic energy close to the core can be an order of magnitude larger than the change in total energy, the total energy error is low [39].

2.5 Crystal structures

A crystal lattice is described by 3 primitive vectors, $a\vec{A}_1 + b\vec{A}_2 + c\vec{A}_3$ where a, b, and c are integers. For each point in this lattice, the basis vectors, $\vec{B}_1$, $\vec{B}_2$, ... $\vec{B}_N$ determine the coordinates relative distance from the lattice points, where atoms of a certain type are placed, denoted C_1, C_2, ... C_M. Atoms of a certain type can have more than one location in a unit cell, so that more than one basis vector can correspond to for example C_1. A cell made of the 3 primitive vectors, with volume $\vec{A}_1 \cdot (\vec{A}_2 \times \vec{A}_3)$, is called a *unit cell*. An example on a lattice is the *diamond* structure shown in Fig. 8:
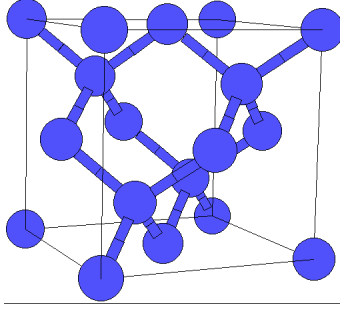
Figure 8: A crystal lattice example, *diamond*.

The primitive vectors for *diamond* are

$$\vec{A}_1 = \frac{1}{2}a\vec{y} + \frac{1}{2}a\vec{z}$$
$$\vec{A}_2 = \frac{1}{2}a\vec{x} + \frac{1}{2}a\vec{z}$$
$$\vec{A}_3 = \frac{1}{2}a\vec{x} + \frac{1}{2}a\vec{y}$$

and the basis vectors for atom C_1 are

$$C_1 \quad : \quad \vec{B}_1 = 0$$
$$C_1 \quad : \quad \vec{B}_2 = \frac{1}{4}a\vec{x} + \frac{1}{4}a\vec{y} + \frac{1}{4}a\vec{z}$$

The unit cell volume V of this structure is

$$V = \vec{A}_1 \cdot (\vec{A}_2 \times \vec{A}_3) = a^3 \left(\frac{1}{2}\vec{y} + \frac{1}{2}\vec{z} \right) \cdot \begin{vmatrix} \hat{x} & \hat{y} & \hat{z} \\ 1/2 & 0 & 1/2 \\ 1/2 & 1/2 & 0 \end{vmatrix} = \frac{1}{4}a^3 \qquad (140)$$

The volume/atom for a crystal is the unit cell volume divided on the number of atoms in the unit cell.

3 Computational details

3.1 Hardware

Njord [40] is a supercomputer with 59 compute nodes, each compute node having a total of 15.2GHz distributed over 8 dual-core processors. Njord is localized in Trondheim. Stallo [41] is a supercomputer with 704 servers, each with two 2.66GHz quad-core processors. Stallo is localized in Tromsø.

3.2 Amsterdam Density Functional [42]

Amsterdam Density Functional is a program package used for calculation of energies and magnetic and electron properties of atomic systems with the DFT method. The molecular orbitals used in the ADF package are a combination of *Slater orbitals* and numerical basis functions. In the ADF package there is a program called "ADF" that is used for molecular calculations, and a program called "BAND" that is used for crystal structure calculations. The reasons for using the package are:

1. It contains many important exchange and correlation functionals.

2. It uses a basis set containing Slater orbitals.

3. The database contains basis sets for atoms up to atom number 118, and 5 different basis sets for each atom to choose between, in addition to the ZORA basis sets.

4. $ZORA_{SO}$ makes it possible to get good results for heavy atoms.

5. In the ADF program, full molecular symmetry is available, including non-Abelian groups as well as Abelian groups.

6. It has all the important approximations, making it possible to calculate complex systems with high accuracy.

7. The CPU time scales fairly well with the number of processors that are working in parallell on a job.

8. As the BAND program and the ADF program are in the same package, there will be better consistency in the input parameters for the force field.

9. To get results consistent with earlier work [8, 9]

10. It contains programs for visualizing the results of ADF and BAND jobs.

The input parameters for the calculation used in the ADF program, ADF2007.01, relevant for this study are

1. What kind of exchange and correlation functional to use.

2. Whether to include Zeroth-Order Regular Approximation.

3. The basis set for the calculation.

4. The frozen core size.

5. Electron wave function (SCF) parameters: Max number of iterations, the wave function convergence criterion.

6. The DIIS procedure; $Mixing$, $DIIS$, and $NEWDIIS$

7. Geometry parameters: Convergence criteria, maximum number of iterations.

8. An accuracy parameter for the numerical integration called $INTEGRATION$.

9. The type of atoms and their positions.

10. Whether to include spin and charge parameters: restricted vs. unrestricted, collinear vs. noncollinear.

11. Whether to use ordinary molecular symmetry.

The input parameters for the calculation used in the BAND program, BAND2007.01, relevant for this study are

1. What kind of exchange and correlation functional is NOT used as input parameter in BAND2007.01. The program calculates the electron density by only using LDA exchange and correlation functional, and then calculates all the GGAs for that density.

2. Whether to include Zeroth-Order Regular Approximation.

3. The basis set for the calculation.

4. Frozen core size.

5. Two parameters for the accuracy of the integrals, called $ACCURACY$ and $KSPACE$.

6. The zero overlap criterion, called *Dependency basis*.

7. The crystal lattice used, i.e., the primitive vectors and basis vectors for atoms.

3.2.1 DIIS procedure

For getting the electron wavefunctions for a given geometry to converge, one has to run several cycles for optimizing the electron density, as shown in section 2.3.9. To speed-up convergence and to avoid non-convergent oscillatory behavior, the electron wavefunctions at the next cycle are constructed as a mixture of the computed new data and those used in the cycles before. The default setting is to only include the previous cycle. The $DIIS$ (Direct Inversion in the Iterative Subspace) procedure allows the program to include more previous iterations. The electron density can then converge faster and avoid non-convergent oscillatory behavior between iterations. The $DIIS$ procedure starts after 10 cycles as default when $DIIS$ is invoked. $Mixing$ is the relative weight of the new potential, when it is mixed with the potential that was used in the previous cycle, and the default is set to 0.2. $Mixing$ is only used as long as the $DIIS$ procedure is not. The $Mixing$ and the $DIIS$ procedures slow down the convergence, but makes it more stable. The $NEWDIIS$ keyword invokes a $DIIS$ procedure that was newly developed when ADF2007.01 became available.

3.2.2 $ACCURACY$, $KSPACE$, and *Dependency basis*

The parameter $ACCURACY$ gives good results for values above 4.5, and is the value that determines the number of integration points over the densities, along with other variables determining the accuracy of the result. The parameter $KSPACE$ is for the accuracy of integration in k-space, giving good results for values above 3, but should only be chosen as an odd number. *Dependency basis* is the minimum value for the overlap matrix elements (approximating them to 0 when below the minimum value).

3.2.3 Basis sets used in ADF [43]

The basis sets available in ADF are called *Double zeta* (DZ), *Triple zeta one polarization function* (TZP), *Triple zeta two polarization functions* (TZ2P) and *Quadruple zeta four polarization functions* (QZ4P). All the basis sets have a frozen core approximation available. The difference is the complexity of each molecular orbital, being composed by more than one Slater orbital. In the *core region* of DZ, TZP, and TZ2P, the orbitals are composed of two basis functions. Using the expression for Slater type orbitals shown in eq. 119, an example with the 1s orbital is:

$$|1s\rangle = c_1 2\zeta_1^{3/2} e^{-\zeta_1 r} + c_2 2\zeta_2^{3/2} e^{-\zeta_2 r} \tag{141}$$

The QZ4P has three functions in the core region. In the *valence region* DZ has two basis functions, TZP and TZ2P have three basis functions, and QZ4P has four basis functions. In addition, the basis sets differ in the number of extra valence orbitals

they include, going from including the least (DZ) to including the most (QZ4P). For Scalar Relativistic ZORA, extra tight 1s and 2p core orbitals have been included (for heavier atoms) in these basis sets to account for the relativistic effects. For Spin-Orbit ZORA the same extra tight 1s and 2p core orbitals are included, except one has to include orbitals for both spinors $j = l - \frac{1}{2}$ and $j = l + \frac{1}{2}$ (where the lowest j orbitals are filled first). Only s, p, d and f-type spherical harmonics have been used to build the basis sets due to limitations in the ADF program.

3.3   Input parameters for ADF and BAND programs

To be able to make a consistent data set, it is important to use the same input parameters for the ADF simulations as has been done earlier [8, 9]. The choice of energy functional was therefore RPBE, using spin-orbit ZORA. For the crystal structures in this master assignment, the choice in basis set was TZP, and the frozen core size was set to "small". For the BAND program, the $ACCURACY$ and $KSPACE$ parameters were set to 6 and 5 respectively, and $Dependency\ basis$ was set to 10^{-10}. Spin-orbit coupling does not have the ordinary molecular symmetry. Therefore symmetry in the ADF program has to be turned off. Unrestricted spin means that pairs of electrons are *not* in the same orbital with spin in opposite directions if another configuration gives lower energy. The spin is therefore chosen to be unrestricted. If the key *collinear* is used, the magnetization is in one defined direction, while it is not necessarily so with the key *noncollinear*. The key *noncollinear* is therefore used, as the magnetization is not perfectly aligned when using spin-orbit coupling.

4 Methods

4.1 Crystal structures

An important input parameter in ReaxFF is the energy for different crystal structures and corresponding volume for each unit cell in the structure. Some crystal structures for lead, strontium, titanium, and oxygen were calculated, as an addition to earlier calculations [8, 9]. First, the minimum energy for these crystals and the corresponding lattice constant a were found. Then the geometry optimized volume per SrO, per PbSr, and per Pb, V_0, was calculated. The energy was found as a function of the the volume/atoms between 0.5 V_0 and 1.5 V_0, in steps of 0.1 V_0. The crystal structures used in this study are shown in Appendix A. The structures $B1$, $B2$, and $L1_0$ were found for PbSr, the energy as a function of the volume/atoms shown in Fig. 9. The structures $B1$ and $L1_0$ were found for SrO, the energy as a function of the volume/atoms is shown in Fig. 10. The $B2$ crystal structure is also plotted into the figure, as it was computed in Ref. [44]. Data for the α structure for lead was found, without finding the energy minimum first. This structure was primarily made for testing the ReaxFF force field described in section 4.4.

4.2 Molecules

In the ReaxFF force field, the three most important bond-order terms are the bond energy, valence angle energy, and the torsion angle energy. It was therefore necessary to make a data set that imitated these terms. We encountered some convergence problems with geometry optimization methods on many of the molecules consisting of lead, strontium, oxygen, and titanium. Hydrogen atoms were therefore added to these molecules to increase the coordination number for the atoms. The number of bonds were set to 4 for titanium and lead, and 2 for oxygen and strontium. As oxygen was treated as having a negative oxidation state, instead of a positive as was the case for the other atoms, bonds between oxygen and another atoms were treated as a π (double) bond, as often as possible, reducing the number of hydrogen atoms in the molecule by 2. In addition to using hydrogen atoms to satisfy the number of valences, the DIIS procedure was applied. Still, some of the computations have failed to converge for some of the bond lengths, valence angles, and torsion angles. Energy from ADF calculations as a function of bond lengths, valence angles, and torsion angles are shown in Appendix B.

44

4.2.1 Bond length

First, the equilibrium geometry for molecules consisting of two heavy atoms and hydrogen atoms was found. Then the bond lengths between the two heavy atoms were varied, using a constricted geometry optimization per step. We found parameters for 7 molecules in total, though some of them would not converge for all bond lengths. The molecules that were used are shown in table 4. Energy from ADF calculations as a function of the O-O distance in the O_2 molecule is illustrated in Fig. 12. As the distance approaches infinity, the energy should approach the sum of the energy of the two resulting fragments. As this fragment energy is important in ReaxFF, it was important to calculate the energy of single atoms/atom groups, shown in table 5, as well as it was important to confirm how many hydrogen atoms were bonded to each of the heavy atoms in the fragment. By looking at the distance-energy plots in Appendix B, it was concluded that the energies would go towards values given in table 6 when the distances would get large. The number of hydrogen atoms bonded to each heavy atom was confirmed by using a grapical user interface, $adfview$.

4.2.2 Valence angle

First, the geometry was optimized for molecules consisting of three heavy atoms and a number of hydrogen atoms. Then the valence angle of the three heavy atoms was varied, using constricted geometry optimization for each step. For molecules with high computational time, meaning more than 10 hours for finding the energy minimum, fewer geometries were found parameters for. The energy minimization for three-atom molecules did not converge for all the different atom configurations. Some of the optimized molecules were triangle-shaped with only sharp angles. These were not used because it would not be a good description of the valence angle at the energy minimum when atom a_1 and a_3 in the a_1-a_2-a_3 structure were bonded to each other. A total of 9 molecules were found valence angle parameters for. Table 7 gives an overview over the valence angles that were used/were not used. Energy from ADF calculations as a function of the valence angle Pb-O-O is shown in Fig. 13.

4.2.3 Torsion angle

Parameters were found for torsion angles a_1-a_2-a_3-a_4, where a_2 and a_3 were Sr, Ti, Pb, and O, with a number of hydrogen atoms bonded to them. Only hydrogen atoms were used as atom a_1 and a_4, because this assignment would be too large otherwise; those systems were already found equilibrium geometries for, the systems with less heavy atoms would converge faster and have less chances of failing to converge. As the symmetry repeats itself after turning 60 degrees for molecules with three hydrogen atoms bonded to a_2 or a_3, the torsion angle was only varied that much. As hydrogen

peroxide only has one hydrogen atom bonded to each oxygen atom, it was needed to turn that angle 180 degrees. Energy from ADF calculations as a function of the torsion angle H-Pb-O-H is shown in Fig. 14.

4.3   Computational time

To give an idea of the computational resources needed for ADF and BAND calculations, some of the crystal structures and molecules used in the calculations are displayed in table 9. All computations in the table were done using Stallo, with 2 servers per computation.

4.4   The process of making a ReaxFF force field for lead, using lead crystals as data set

The procedure for making a force field was done according to section 2.2.7. No ReaxFF force field have been made for lead before, so the initial values for the constants in the ffield file were guessed, based on values for other atoms parametrized in ReaxFF, except for the number of valences, which was set to 4. The data set was collected from work done in Ref. [9], and consisted of crystal structures for lead, calculated with the RPBE functional with $ZORA_{SO}$. The crystal structures were FCC, BCC, SC, HCP, and $diamond$ (Appendix A has an overview of these). The first attempt to make a satisfactory force field failed to match the data set used for making it. This is seen by comparing between crystal structures produced by the force field, Fig. 15 and the data set, Fig. 17. Because the $diamond$ structure fit worst with the data set, another force field was made without using $diamond$. The results for that force field are illustrated in Fig. 18. This force field is from here on refered to as the "Gaute force field". The fort.99 file belonging to that force field is shown in Fig. 16. The figure shows which energies were used for optimizing the force field, in addition to the weight for each of these energies. The weight was set to 0.1 for the relative minima between the structures, and because SC was more stable for 3.50 Å than for 3.37 Å which was the energy minimum for DFT calculations, 3.50 Å was used to compare relative minima for that crystal. The weight value was high where the energy derivative was high, because one can still get a good result with larger deviations in those areas. As a reminder of the expression for calculating the error, eq. 40 is repeated as eq. 142.

$$ERROR = ([ffieldenergy - datasetvalue]/weight)^2 \qquad (142)$$

To be able to say something about the transferability of the ReaxFF force field, energies for different geometries were found for the $diamond$ structure, the α structure,

46

and the Pb-Pb molecule with the ReaxFF force field, as said geometries would be compared to DFT calculations of the same systems. The *diamond* structure and the α structure are included into Fig. 18. The energy for the Pb$_2$ molecule as a function of the interatomic distance is displayed in Fig. 19, using both the ReaxFF force field and data set values.

5   Results
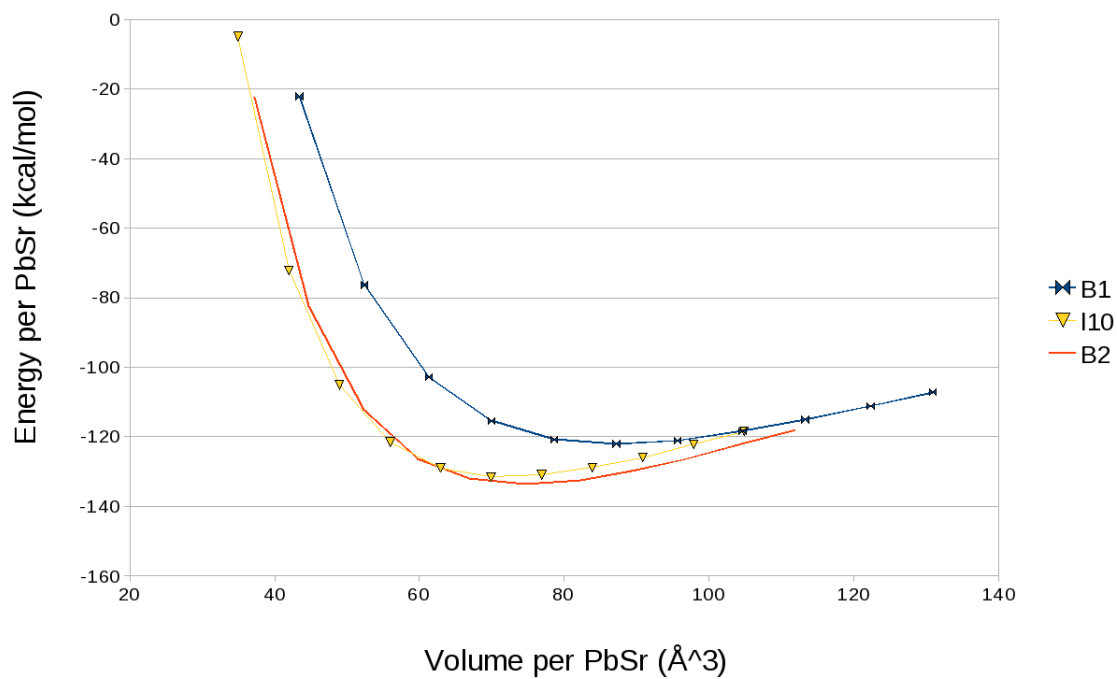
Figure 9: Energy from ADF calculations as a function of the volume per PbSr for PbSr crystal structures. The crystal structures are explained in Figs. 28-30.
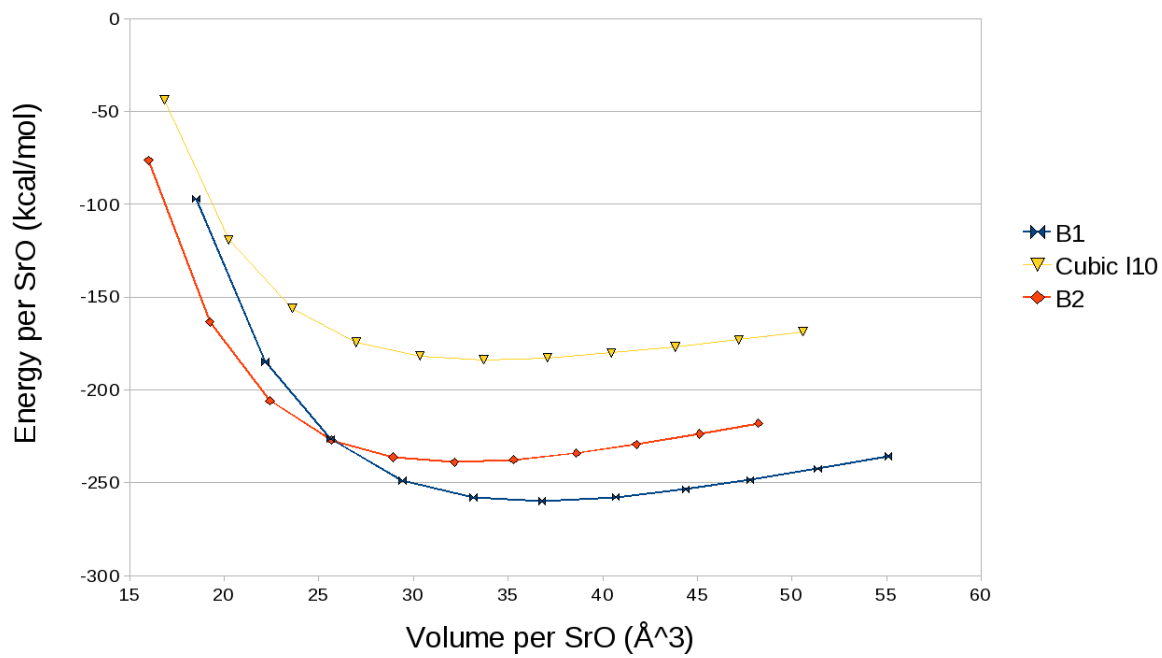
Figure 10: Energy from ADF calculations as a function of the volume per SrO for SrO crystal structures. Data for $B2$ is found from Ref. [44]. The crystal structures are explained in Figs. 28-30.
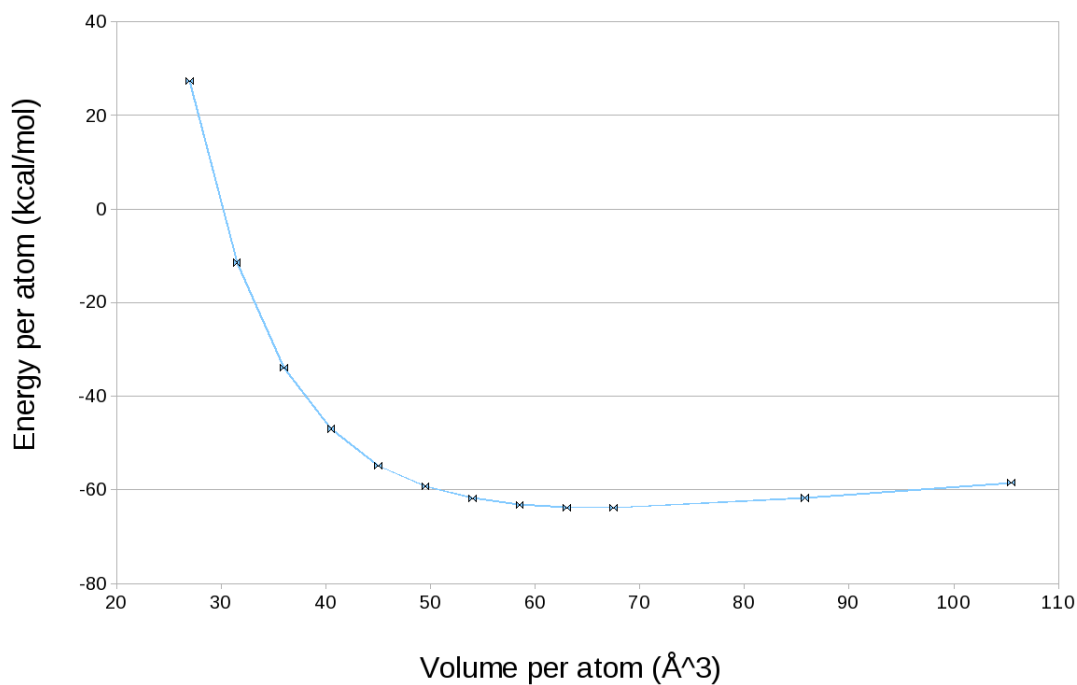
Figure 11: Energy from ADF calculations as a function of the volume per atom for Pb α structure. The crystal structure is explained in Fig. 33.

Table 4: Molecules used for finding bond stretch energies. d= distance, measured between the two atoms, and is measured in Å. The energy as functions of the distance are displayed in Figs. 34-40, and the corresponding molecules are illustrated in Figs. 55-60.

Bond	Hydrogen	Equilibrium d.	Min. d.	Max. d.
Pb-Pb	Pb_2	3.00	2.05	3.95
Pb-Pb	PbH_3PbH_3	2.95	2.05	4.45
Pb-O	PbH_2O	1.95	1.35	3.15
Pb-Sr	PbSr	3.35	2.35	5.65
Pb-Ti	PbTi	2.79	1.95	3.75
O-O	O_2	1.24	0.84	1.84
O-O	OHOH	1.49	1.04	2.14
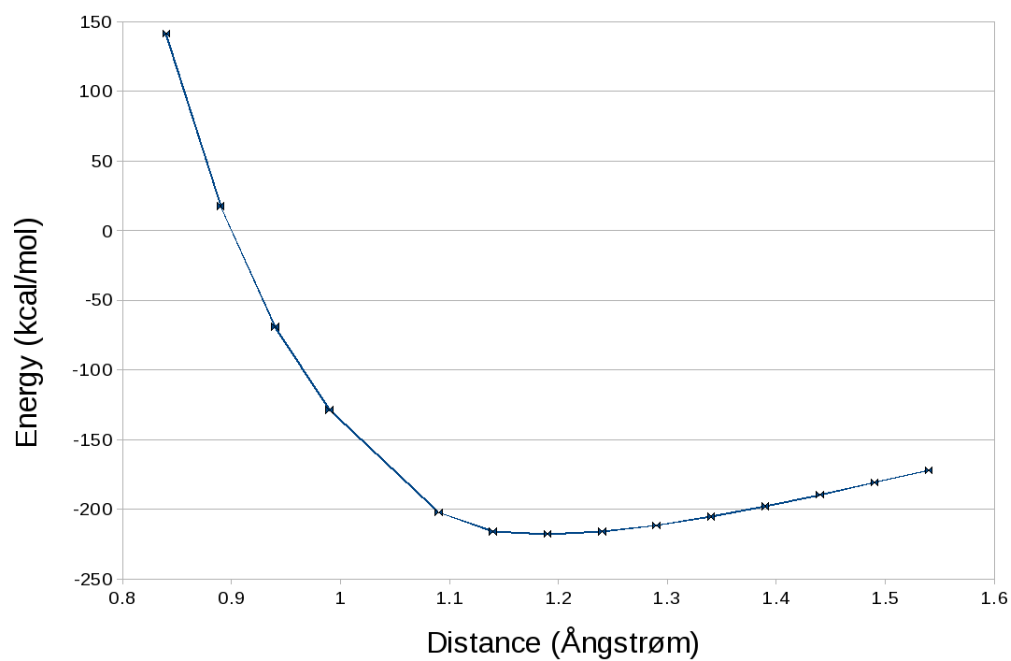
Figure 12: Energy from ADF calculations as a function of the interatomic distance in the O_2 molecule.

Table 5: Energies for atoms/molecules used in bond length parametrizations. Titanium did not converge.

Atom/molecule	Energy (kcal/mol)
O	-45.06
OH	-174.67
Pb	-96.06
Ti	no convergence
Sr	-2.98
PbH_2	-248.77
PbH_3	-305.25

Table 6: The energy for infinite distance between atoms. Because the single point energy for titanium did not converge, there are no energy value for 'Pb + Ti'

Atoms/molecules	Energy (kcal/mol)
PbH_3 + PbH_3	-610.50
PbH_2 + O	-293.83
O + O	-90.12
OH + OH	-349.34
Pb + Pb	-192.12
Pb + Ti	no value
Pb + Sr	-99.04

51

Table 7: Molecules used for finding valence angle energies. v = Valence angle. The angles are measured in degrees. "High comp. cost" means the computation to find energy minimum took more than 10 hours, so the number of computations is decreased. "triangle" means that the three atoms form a triangle with only sharp angles, and therefore the valence angle is not calculated. "hydrogen bridge" refers to two atoms are bonded to one hydrogen. Why this is a problem is explained in section 6.1.1. The energy as a function of the valence angles are displayed in Figs. 41 - 49, and the corresponding molecules are illustrated in Figs. 62-70.

Valence Angle	Molecule	Eq. v.	Min. v.	Max. v.	Comment
Pb-O-O	PbH_3OOH	105	90	175	no problem
Pb-O-Pb	PbH_3OPbH_3	-	-	-	hydrogen bridge
Pb-O-Sr	PbH_3OSrH	165	115	180	no problem
Pb-O-Ti	PbH_3OTiH_3	153	115	175	no problem
Pb-Pb-O	PbH_3PbHO	125	105	145	high comp. cost
Pb-Pb-Pb	$PbH_3PbH_2PbH_3$	114	95	135	high comp. cost
Pb-Pb-Sr	PbH_3PbH_2SrH	-	-	-	triangle
Pb-Pb-Ti	$PbH_3PbH_2TiH_3$	109	90	150	high comp. cost
Pb-Sr-O	PbH_3SrOH	137	90	180	no problem
Pb-Sr-Pb	PbH_3SrPbH_3	130	115	145	high comp. cost
Pb-Sr-Sr	PbH_3SrSrH	-	-	-	failed to converge
Pb-Sr-Ti	PbH_3SrTiH_3	-	-	-	failed to converge
Pb-Ti-O	PbH_3TiHO	-	-	-	failed to converge
Pb-Ti-Pb	$PbH_3TiH_2PbH_3$	105	95	125	high comp. cost
Pb-Ti-Sr	PbH_3TiH_2SrH	-	-	-	triangle
Pb-Ti-Ti	$PbH_3TiH_2TiH_3$	-	-	-	triangle
Sr-Pb-Sr	$SrHPbH_2SrH$	-	-	-	triangle
Sr-Pb-Ti	$SrHPbH_2TiH_3$	-	-	-	triangle
Sr-Sr-Sr	$SrHSrSrH$	-	-	-	failed to converge
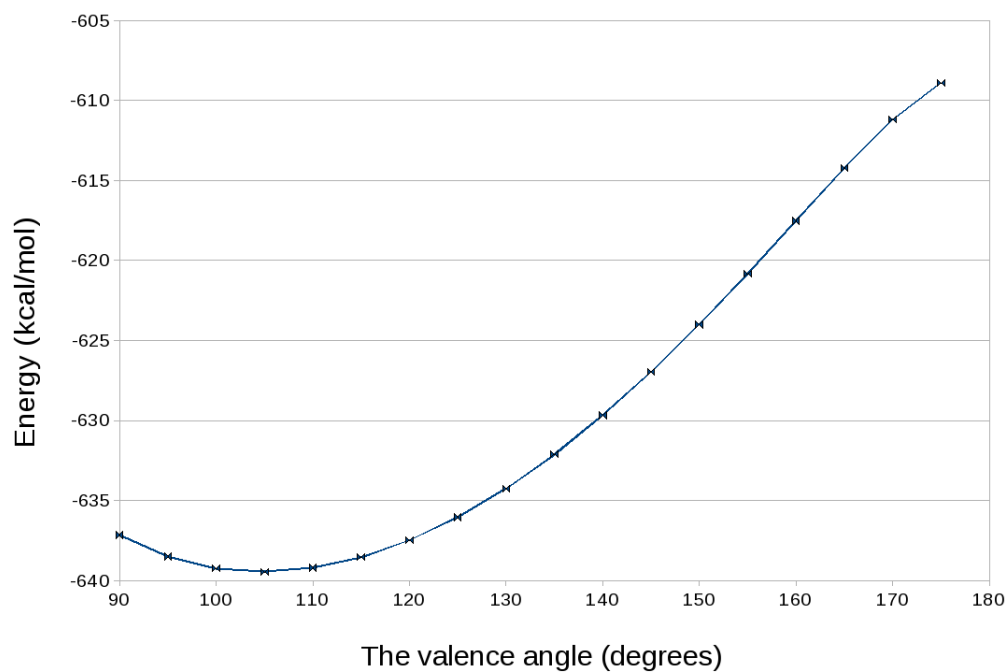
Figure 13: Energy from ADF calculations as a function of the valence angle Pb-O-O. The energy is found by using a start angle of 90 degrees, and increasing it in steps of 5 degrees, doing a constrained geometry optimization for each step. The molecule is illustrated in Fig. 66.

Table 8: Molecules used for finding torsion angle energies. The angle is in units of degrees. The energy as a function of the torsion angles are displayed in Figs. 50-54. The molecules are illustrated in Figs. 55, 59, 60, 71, and 73.

Torsion angle	Molecule	Equilibrium angle.	Minimum angle	Maximum angle
H-Pb-Pb-H	PbH_3PbH_3	60	0	60
H-Pb-O-H	PbH_3OH	60	0	120
H-Pb-Sr-H	PbH_3SrH	110	60	120
H-Pb-Ti-H	PbH_3TiH_3	0	60	120
H-O-O-H	OHOH	82	0	180
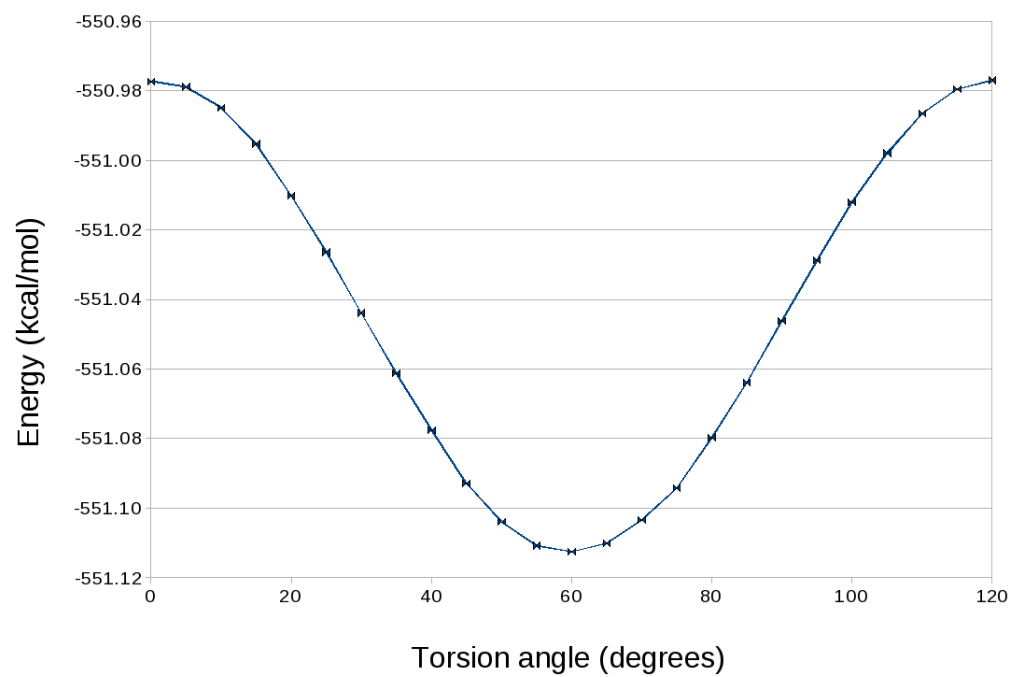
Figure 14: Energy from ADF calculations as a function of the torsion angle H-Pb-O-H in the PbH$_3$OH molecule. The molecule is illustrated in Fig. 71.

Table 9: Computational cost of different geometries. All ADF jobs were done using Stallo, each job using 2 servers (2 processors per server, 2.66 GHz per processor). The time is given in seconds, T = time. T/cycle = time per geometry optimization cycle. In T/cycle, the time is an average over all geometry cycles. *: This computation is done in Ref. [44]. N/A = the geometry is set, so there is no geometry optimization.

Structure	Description	T. elapsed	T/cycle
O_2	single point energy	33	N/A
PbH_3	geometry optimization	1693	81
PbH_3PbH_3	geometry optimization	6565	298
TiH_3TiH_3 *	geometry optimization	43412	190
PbH_3SrOH	geometry optimization	33957	361
PbH_3SrTiH_3	geometry optimization	155254	1438
PbH_3SrTiH_3	geometry optimization	99754	1008
PbH_3PbH_3	Pb-Pb distance set to 2.05 Å	14758	351
PbH_3PbH_3	Pb-Pb distance set to 2.15 Å	7180	378
PbH_3PbH_3	Pb-Pb distance set to 5.05 Å	7843	1120
$PbH_3PbH_2PbH_3$	Pb-Pb-Pb angle at 95 degrees	26890	1120
$PbH_3PbH_2PbH_3$	Pb-Pb-Pb angle at 100 degrees	22606	1076
$PbH_3PbH_2PbH_3$	Pb-Pb-Pb angle at 135 degrees	4775	796
SrO cubic $l1_0$ crystal	lattice constant set to 300	5309	N/A
SrO cubic $l1_0$ crystal	lattice constant set to 303	5847	N/A
SrPb cubic $l1_0$ crystal	lattice constant set to 520	19532	N/A
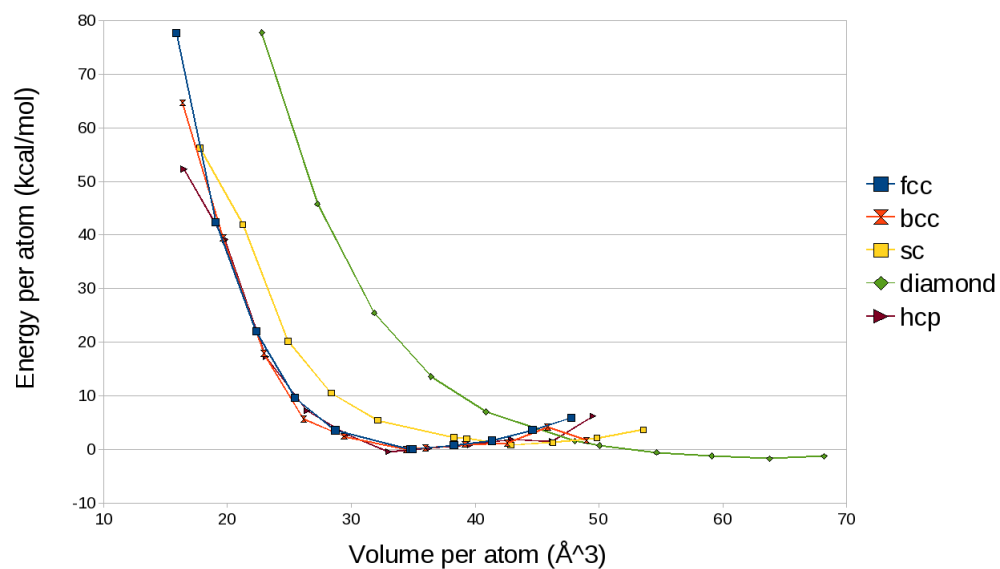
Figure 15: The ReaxFF energy as a function of the volume/atom for *FCC*, *BCC*, *SC*, *HCP*, and *diamond*, the force field is fit to *FCC*, *BCC*, *SC*, *HCP*, and *diamond* lead crystals from ADF calculations. The crystal structures are explained in Figs. 23-27.

```
                                FFfield value QM/Lit value   Weight      Error    Total error
Energy +pb_fcc_5.18/   4 -pb_hcp_3.55/  2     -0.0711       -0.0300     0.1000     0.1687        0.1687
Energy +pb_fcc_5.18/   4 -pb_sc_3.50/   1     -1.4564       -2.6400     0.1000   140.0926      140.2613
Energy +pb_fcc_5.18/   4 -pb_bcc_4.10/  2     -0.1804       -0.6900     0.1000    25.9729      166.2342
Energy +pb_bcc_4.10/   2 -pb_bcc_3.20/  2   -107.6211      -85.4900    15.0000     2.1768      168.4111
Energy +pb_bcc_4.10/   2 -pb_bcc_3.40/  2    -39.6057      -39.9500     5.0000     0.0047      168.4158
Energy +pb_bcc_4.10/   2 -pb_bcc_3.58/  2    -16.1675      -17.7000     2.0000     0.5872      169.0030
Energy +pb_bcc_4.10/   2 -pb_bcc_3.74/  2     -4.7133       -7.1200     1.0000     5.7924      174.7953
Energy +pb_bcc_4.10/   2 -pb_bcc_3.89/  2     -1.8039       -2.0200     1.0000     0.0467      174.8420
Energy +pb_bcc_4.10/   2 -pb_bcc_4.16/  2     -0.1648       -0.3500     1.0000     0.0343      174.8763
Energy +pb_bcc_4.10/   2 -pb_bcc_4.28/  2     -0.7625       -1.2900     1.0000     0.2783      175.1546
Energy +pb_bcc_4.10/   2 -pb_bcc_4.40/  2     -2.2564       -2.7700     1.0000     0.2638      175.4183
Energy +pb_bcc_4.10/   2 -pb_bcc_4.51/  2     -4.6241       -4.7200     1.5000     0.0041      175.4224
Energy +pb_bcc_4.10/   2 -pb_bcc_4.61/  2     -6.7002       -6.5200     2.0000     0.0081      175.4305
Energy +pb_fcc_5.18/   4 -pb_fcc_3.99/  4   -132.9837      -99.2800    15.0000     5.0486      180.4792
Energy +pb_fcc_5.18/   4 -pb_fcc_4.24/  4    -45.7520      -47.2000     5.0000     0.0839      180.5630
Energy +pb_fcc_5.18/   4 -pb_fcc_4.47/  4    -19.6810      -21.6000     2.0000     0.5468      181.1099
Energy +pb_fcc_5.18/   4 -pb_fcc_4.67/  4     -8.3915       -8.8900     1.0000     0.2485      181.3583
Energy +pb_fcc_5.18/   4 -pb_fcc_4.87/  4      0.1501       -2.8800     1.0000     9.1814      190.5397
Energy +pb_fcc_5.18/   4 -pb_fcc_5.19/  4     -0.0266       -0.0300     1.0000     0.0000      190.5398
Energy +pb_fcc_5.18/   4 -pb_fcc_5.35/  4     -0.6379       -1.0200     1.0000     0.1460      190.6858
Energy +pb_fcc_5.18/   4 -pb_fcc_5.49/  4     -1.8830       -2.4600     1.0000     0.3330      191.0187
Energy +pb_fcc_5.18/   4 -pb_fcc_5.63/  4     -4.2570       -4.1000     1.5000     0.0110      191.0297
Energy +pb_fcc_5.18/   4 -pb_fcc_5.76/  4     -6.5860       -6.2200     2.0000     0.0335      191.0632
Energy +pb_sc_3.37/    1 -pb_sc_2.61/   1    -94.1408      -83.4000    15.0000     0.5127      191.5759
Energy +pb_sc_3.37/    1 -pb_sc_2.77/   1    -33.8353      -39.3900     5.0000     1.2342      192.8101
Energy +pb_sc_3.37/    1 -pb_sc_2.92/   1    -15.5499      -17.2800     2.0000     0.7483      193.5584
Energy +pb_sc_3.37/    1 -pb_sc_3.05/   1     -7.3859       -6.9600     1.0000     0.1814      193.7398
Energy +pb_sc_3.37/    1 -pb_sc_3.18/   1     -2.8423       -1.9100     1.0000     0.8692      194.6090
Energy +pb_sc_3.37/    1 -pb_sc_3.40/   1      0.1741       -0.2200     1.0000     0.1553      194.7644
Energy +pb_sc_3.37/    1 -pb_sc_3.50/   1      0.8223       -1.1900     1.0000     4.0492      198.8136
Energy +pb_sc_3.37/    1 -pb_sc_3.59/   1      0.5577       -2.5000     1.0000     9.3497      208.1633
Energy +pb_sc_3.37/    1 -pb_sc_3.68/   1     -0.3046       -4.1200     1.5000     6.4700      214.6333
Energy +pb_sc_3.37/    1 -pb_sc_3.77/   1     -2.0320       -6.0700     2.0000     4.0763      218.7097
Energy +pb_hcp_3.55/   2 -pb_hcp_2.82/  2   -103.5113      -83.2100    15.0000     1.8317      220.5414
Energy +pb_hcp_3.55/   2 -pb_hcp_2.99/  2    -39.5191      -39.2300     5.0000     0.0033      220.5448
Energy +pb_hcp_3.55/   2 -pb_hcp_3.15/  2    -15.6309      -16.8600     2.0000     0.3777      220.9224
Energy +pb_hcp_3.55/   2 -pb_hcp_3.30/  2     -6.4571       -6.0900     1.0000     0.1348      221.0572
Energy +pb_hcp_3.55/   2 -pb_hcp_3.43/  2     -2.1878       -1.6500     1.0000     0.2892      221.3464
Energy +pb_hcp_3.55/   2 -pb_hcp_3.66/  2     -0.2450       -0.2200     1.0000     0.0006      221.3470
Energy +pb_hcp_3.55/   2 -pb_hcp_3.77/  2     -0.8596       -1.5000     1.0000     0.4102      221.7572
Energy +pb_hcp_3.55/   2 -pb_hcp_3.87/  2     -2.1032       -3.2000     1.0000     1.2030      222.9602
Energy +pb_hcp_3.55/   2 -pb_hcp_3.97/  2     -4.5407       -5.0300     1.5000     0.1064      223.0667
Energy +pb_hcp_3.55/   2 -pb_hcp_4.06/  2     -6.5867       -7.2300     2.0000     0.1034      223.1701
```

Figure 16: The fort.99 file for the Gaute force field. For an explanation of the columns in the file, see Fig. 7.
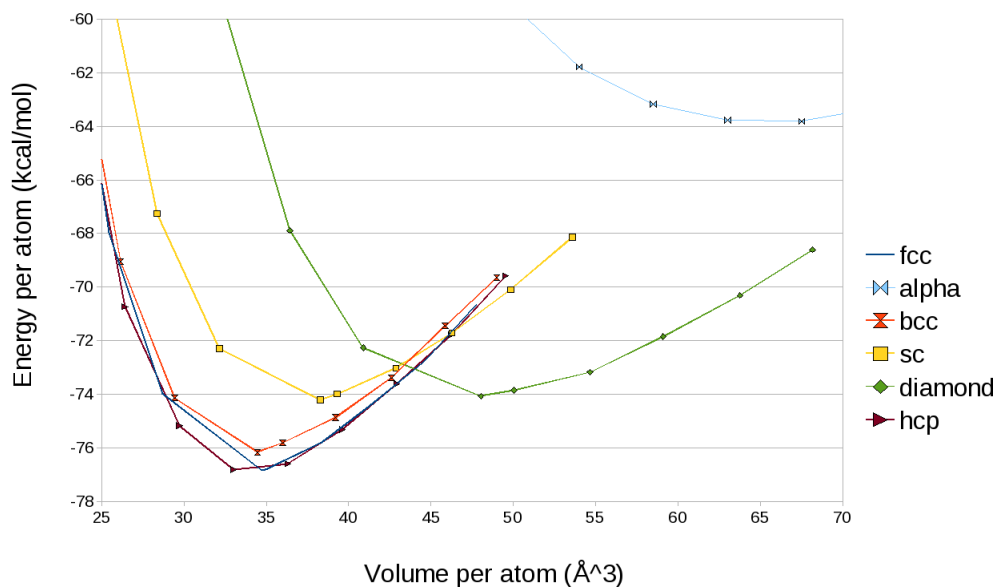
Figure 17: Energy from ADF calculations as a function of the volume/atom for Pb crystal structures. Energies for *FCC*, *BCC*, *HCP*, *SC*, and *diamond* are found from Ref. [9]. The crystal structures are explained in Figs. 23-27 and 33.
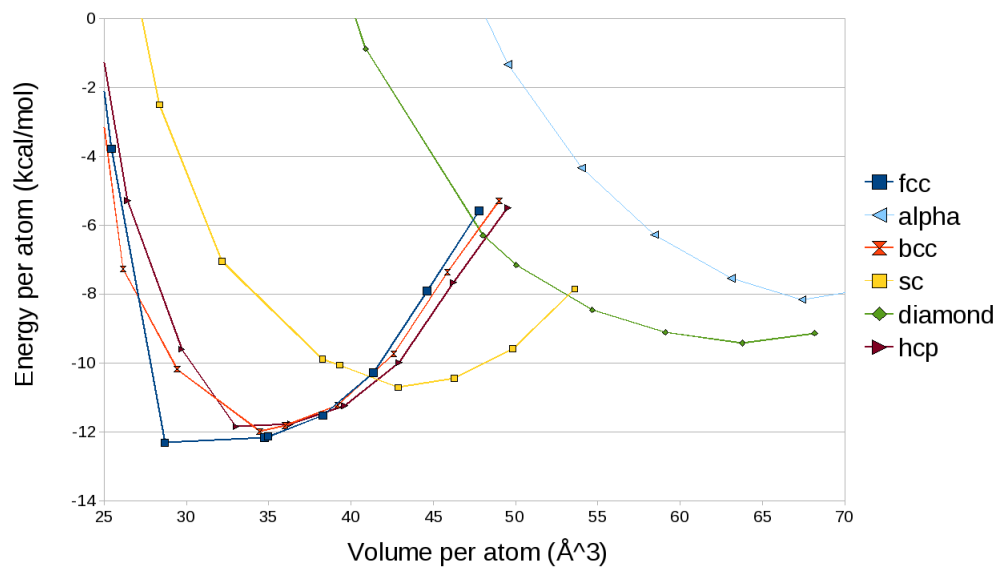
Figure 18: The Gaute force field energy, denoted ReaxFF in this figure, as a function of the volume/atom for lead lattices. The crystal structures are explained in Figs. 23-27 and 33.
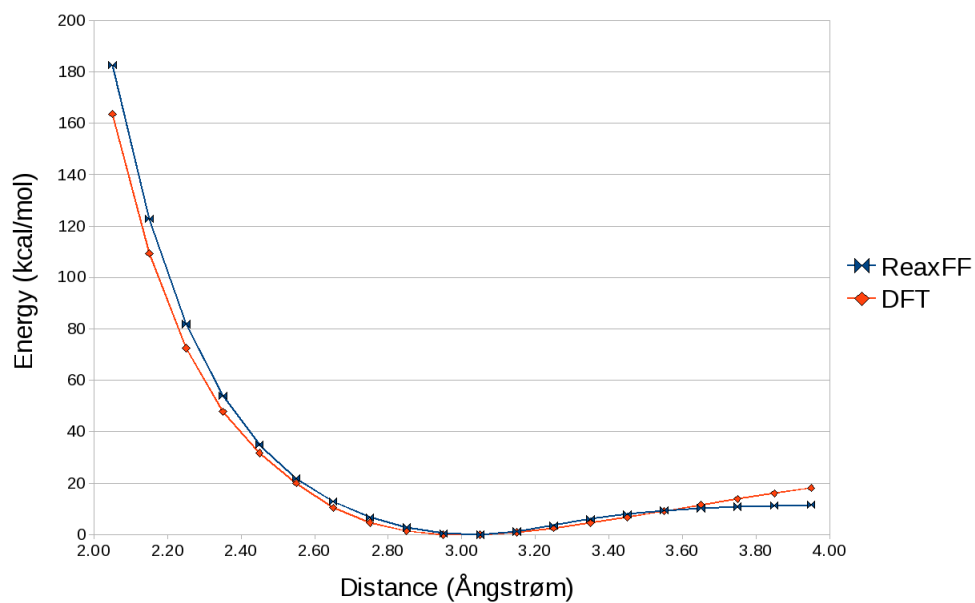
Figure 19: The Gaute force field energy, denoted ReaxFF in this figure, as a function of the Pb-Pb bond distance for Pb_2, plotted against the same molecule calculated with ADF. The bond distances for the energy minima are very close to each other. The largest deviation between the plots is the binding energy, dvs. $2E(Pb) - E_{eq}(Pb_2)$.

Figure 20: The Gaute force field energy, denoted ReaxFF in these figures, as a function of the volume/atom for different lattices, compared to lattices computed with ADF. The V_0 energy for FCC has been set to 0 for both Gaute force field and ADF plots, and the energies in the other lattices have been scaled according to that energy. The crystal structures are explained in Figs. 23-27 and 33.
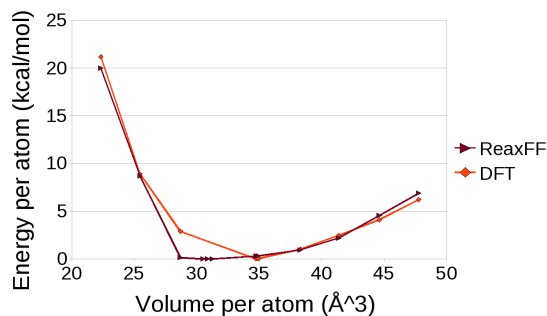
(a) The FCC lattice
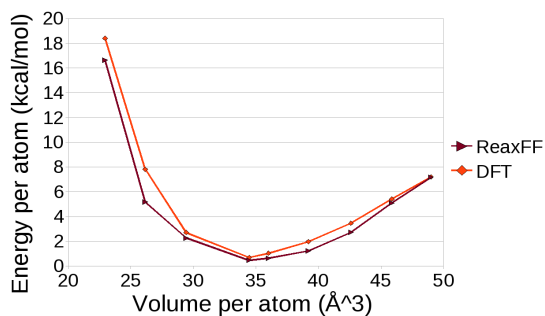
(b) The BCC lattice
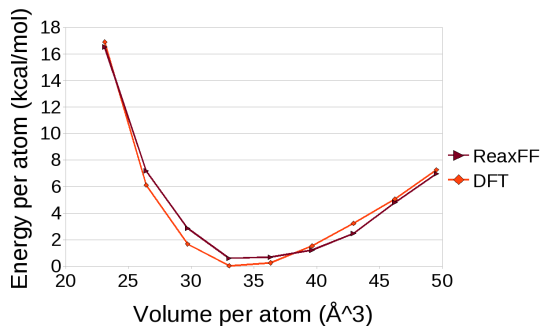
(c) The HCP lattice
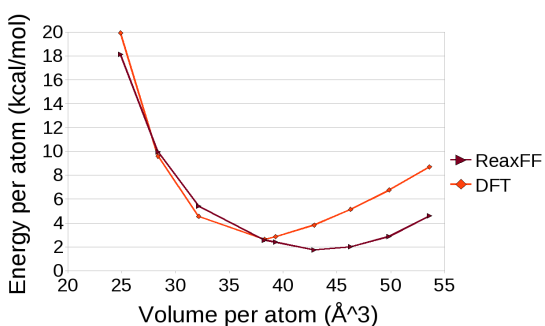
(d) The SC lattice
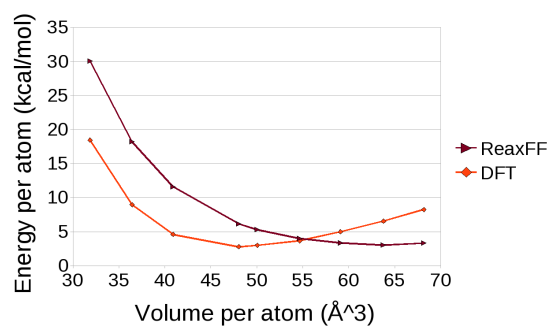
(e) The $diamond$ lattice
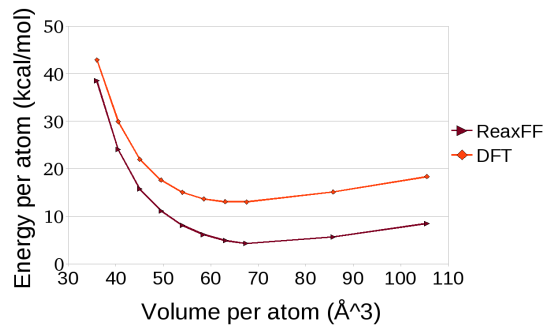
(f) The α lattice

6 Discussion

6.1 ADF

6.1.1 Excluded results

Inspection of the molecular structures in the graphical user interface, *adfview*, shows that different unwanted geometries have taken place for some of the fixed bond lengths/valence angles/torsion angles for some of the molecules. Unwanted geometries are geometries that does not describe the bond length, valence angle, or torsion angle. In these cases, the computations cannot be used:

- When an interatomic distance for a bond in the valence angle or torsion angle is much larger than it is for other systems (a bond is broken).

- When a hydrogen atom is bound to more than one heavy atom. Because hydrogen is not meant to be part of the resulting force field, it would be too much work to include a_1-H-a_3 interactions in the ReaxFF force field, and therefore those terms should be avoided.

Not usable geometries are excluded from the plots in Appendix B.

6.1.2 Numerical integration errors

Some displacements in the energy have been caused by numerical integration errors, and the size of these errors varies between different systems. Fig. 21 shows that the lattice constant for the minimum of the cubic $l1_0$ structure may be displaced a few pm, and maybe 0.01 or 0.02 kcal/mol.
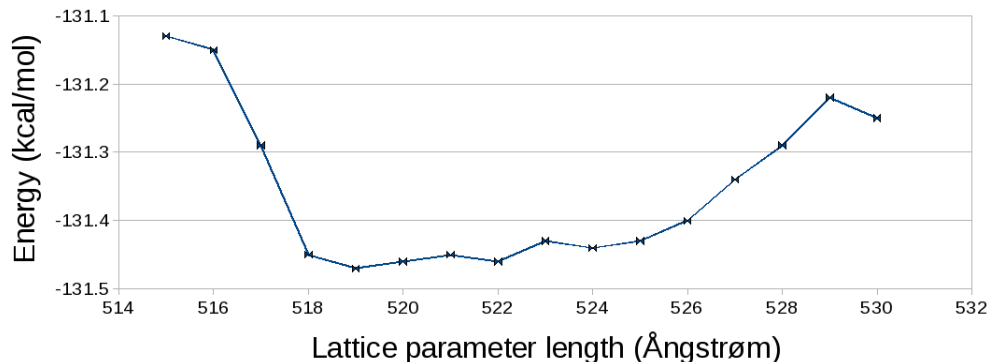
Figure 21: Energy as a function of the lattice constant for a PbSr cubic $l1_0$ structure around the energy minimum at 5.19 Å. The uneven nature of the plot is due to numerical integration errors.

61

The numerical integration error varies from system to system. The only ADF-plot where the numerical integration error is possible to see is the plot for the H-Pb-Sr-H torsion angle, Fig. 54, where the energy scale is very small.

6.1.3 The CPU time

As can be seen from table 9, the cpu-time differs a lot for different structures. Three points worth noticing from looking at the table are:

- As to be expected, the cpu-time is much greater for large systems than for small systems.

- By comparing PbH_3PbH_3 and TiH_3TiH_3, it is shown that systems containing more electrons are not necessarily the systems that takes the longest time to optimize. This is due to a much slower geometry convergence for TiH_3TiH_3 (229 geometry cycles, versus 22 for PbH_3PbH_3).

- The time for one constricted geometry optimization varies for the same set of atoms for different aimed geometries.

6.2 The Gaute force field

A few plots have been made for comparing computations done with Gaute force field and computations done with ADF: Fig. 18, Fig. 17, Fig. 19, and Fig. 20. By studying these plots, some weaknesses in the force field can be mentioned:

- The equilibrium geometry is displaced for some of the systems, specially *diamond* and *SC*, while other systems such as *BCC* and *HCP* fit very well, showing more work is needed to be able to make a good force field.

- Fig. 17 shows that the bonding energy for Pb-Pb is much less when using the ReaxFF force field than when using ADF results. This could also be the case for the crystal lattices, but to be able to say more about this, ADF and ReaxFF computations for larger lattice constants are needed.

- Fig. 17 shows a good fit for all Pb-Pb energies when the bond is not close to breaking. This indicates that the transferability of the force field might be good.

Possible reasons the force field is not better:

- Details in making the force field. As mentioned above, a bigger data set is needed. The weighting of different terms in trainset.in could also have been unoptimal.

- The energy terms in the force field might not hold for the system, so a new energy term might be needed, and some energy terms might need to be adjusted. This possibility is not explored in this paper, and more work on the force field should be done before exploring this possibility.

A combination of these two reasons is of course plausible.

6.3 The compatibility between results

In this study, and in Ref. [9], all computations for the data set are done with Spin-Orbit ZORA (ZORA$_{SO}$) in the functional. In Ref. [8] and Ref. [44] the computations have been/are conducted by including Scalar Relativistic ZORA (ZORA$_{SR}$). In Ref. [8, 44] the systems do not contain lead atoms, so the heaviest atom is strontium. Data in table 10 are copied from table 2 and 3 in Ref. [8]. The lattice constants used for calculating the volume/atom at energy equilibrium (V$_0$) are shown in the UV columns in table 10, using the average lattice constant from the Eq. geo. column, as the energy minimum is most probably located at that value. In table 11, V$_0$ is calculated from the lattice constants from the UV columns in table 10. The crystal structures are described in Appendix A. Table 11 shows the deviation between ZORA$_{SO}$ and ZORA$_{SR}$ for the volume/atom and the energy at V$_0$.

Table 10: The energies and lattice constants for computations with ZORA$_{SR}$ and ZORA$_{SO}$ for strontium *FCC*, *BCC*, *SC*, and *diamond* lattices. eq. geo. = equilibrium geometry in Ångstrøm, SR = ZORA$_{SR}$, SO = ZORA$_{SO}$, the energy unit is kcal/mol, UV = Used lattice constant Value, for calculating V$_0$ (volume/atom at energy equilibrium) in table 11.

Crystal	Eq. geo. SR	UV	Eq. geo. SO	UV	Energy SR	Energy SO
FCC	6.16-6.17	6.16	6.17	6.17	-32.77	-33.05
BCC	4.87	4.87	4.90	4.90	-32.59	-32.63
SC	3.98	3.98	3.98	3.98	-21.45	-21.48
diamond	10.05-10.06	10.06	9.96-10.02	9.99	-22.51	-22.55

Table 11: Values for strontium lattices: The V$_0$ (volume/atom at energy equilibrium) energy for ZORA$_{SR}$, and the differences in the energy and V$_0$ for ZORA$_{SO}$ − ZORA$_{SR}$. ZORA$_{SO}$ − ZORA$_{SR}$ = Δ.

Crystal	V$_0$ for ZORA$_{SR}$ (Å^3)	Δ V$_0$ (Å^3)	ΔV$_0$/V$_0$	Δ Energy (kcal/mol)
FCC	58.72	0.285	0.0049	-0.28
BCC	57.75	1.074	0.0186	-0.04
SC	63.04	0	0.0000	-0.03
diamond	127.26	-2.638	-0.0207	-0.04

The relative volume/atom error, $\Delta V_0/V_0$, is largest for *diamond*. To find out how large that error is, the relative error is applied to the *diamond* crystal structure for lead, showing the original *diamond* structure, and the *diamond* structure displaced -0.0207 volumes/atom and -0.04kcal/mol in Fig. 22(a). In Fig. 22(b) the FCC structure is displaced accordingly, because FCC has the largest energy error. One should keep in mind that the energy displacement might not be the same for all volumes/atom for an ADF computation.
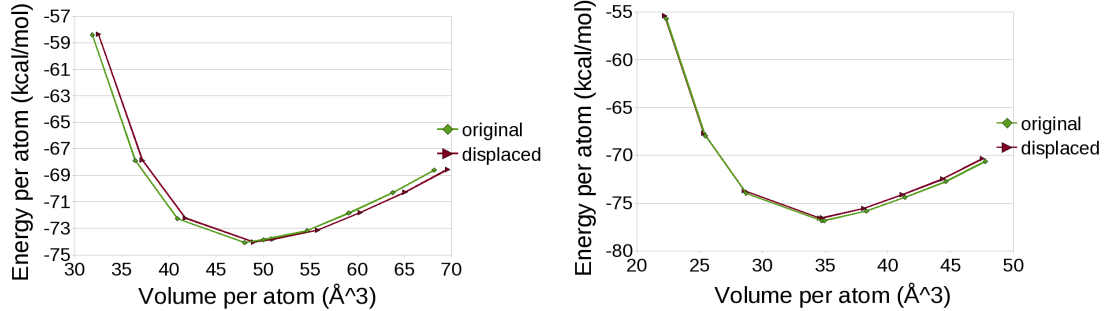
(a) The *diamond* structure, and the same structure displaced -0.04 kcal/mol and -0.0207 volumes/atom.

(b) The FCC structure, and the same structure displaced -0.28 kcal/mol and 0.0049 volumes/atom

Figure 22: Energy as a function of the volume/atom for lead *diamond* and FCC structure, found for ADF with ZORA$_{SO}$, and the same *diamond* and FCC structures with a displacement in energy and volume/atom.

When looking at Figs. 22(a) and 22(b), it is clear that the error from using ZORA$_{SR}$ rather than ZORA$_{SO}$ in the ADF functional for strontium is significant, although the error is smaller than the differences in Fig. 20. A more thorough investigation should be conducted on the matter, as the test conducted here is artificial, as V_0 for ZORA$_{SR}$ was used to construct the whole energy plot. Because relativistic effects in titanium are smaller, as it has atomic number 22, while strontium has 38, ZORA$_{SR}$ probably suffices calculations on titanium.

7 Summary

We have now run density functional theory calculations on different geometries for crystals and molecules, focused on finding parameters for a data set for lead, strontium, titanium, and oxygen. More precisely, we have run calculations for 2 SrO crystals, 3 PbSr crystals, and 1 Pb crystal for different lattice constants. The plots for theenergy as a function of the volume/atoms are shown in Figs. 9-11. We have run calculations on different bond lengths of 7 molecules, on different valence angle of 9 molecules, and on different torsion angle of 5 molecules. The plots for the energy as a function of the bond length/valence angle/torsion angle are shown in Figs. 34-54 Appendix B. This study is not the only study focused on finding parameters for the data set. By adding results from Ref. [8], Ref. [9], and Ref. [44], parameters have been found for for 9 bond lengths, 14 valence angles, 8 torsion angles, and 43 crystal structures. Computations from Ref. [8] and [44] have, however, been done using Scalar Relativistic ZORA, and there is a possibility the results for systems including strontium are not good enough for the data set. We have made a ReaxFF force field for lead, given the name 'Gaute force field', that is fitted to energies of FCC, HCP, SC, and BCC from the data set. When comparing the energy-volume plots for geometries found with the ADF method to the same geometries made by the force field, it is shown that the force field matches well for some of the geometries, and less well for others. Comparing energies for Pb_2 bond stretch values shows that the transferability of the force field might be good.

8   Further work

Based on this study, some suggestion at what to work on in the future are mentioned:

- It is necessary to find more parameters for the data set. Torsion angle data is needed. Data for higher lattice constants might also be necessary to find, as it currently is hard to say anything about good the force field fits for high lattice constants.

- It might be necessary to evaluate strontium parameters for the data set found by using $ZORA_{SR}$, as explained in section 6.3.

- It is necessary to continue building the Pb-Sr-Ti-O ReaxFF force field. This work includes making a geo file that contains all the geometries from the data set, making a trainset.in file with corresponding parameters for the geometries, making a ffield and a params file, and optimizing the force field.

- When the force field is finished it should be used to study the $PbTiO_3$ tetragonal perovskite film on the $SrTiO_3$ cubic perovskite substrate system. As mentioned in section 1.3, this includes looking at $PbTiO_3$ film growth, what happens when the film thickness is decreased, and studying the $PbTiO_3$-$SrTiO_3$ surface more carefully.

- The force field can of course be used for looking at other systems.

- Other atoms can be added to the force field, to be able to look at more systems.

References

[1] W. -Y. Hsu, and R. Raj *Appl. Phys. Lett. 67* **1995** 792-794

[2] Powder Diffraction File, Vol. 35, entity 734 *International Centre for Diffraction data* **1990**

[3] F. Jona, and G. Shirane, Ferroelectric Crystals *Dover Publications, Inc., New York* **1993**

[4] M. Dawber, C. Lichtensteiger, M. Cantoni, M. Veithen, P. Ghosez, K. Johnston, K. M. Rabe and J. M. Triscone *Phys. Rev. Lett. 95* **2005** 177601

[5] G. J. M. Dormans, M. De Keijser, P. K. Larsen *Integrated Ferroelectrics volume 2, issue 1 - 4* **1992** 297

[6] A. T. J. van Helvoort, Ø. Dahl, B. G. Soleim, R. Holmestad, and T. Tybell *App. Phys. Lett. 86* **2005** 092907

[7] M. Sepliarsky, M. G. Stachiotti, and R. L. Migoni *Phys. Rev. Lett. 96* **2006** 137603

[8] K. T. Olsen, Project assignment *Department of Physics, NTNU, Norway* **2008**

[9] G. Oftedal, Project assignment *Department of Physics, NTNU, Norway* **2008**

[10] Kjetil Tesaker Olsen, master grade student *Department of Physics, NTNU, Norway*

[11] A. C. T. van Duin, S. Dasgupta, F. Lorant, and W. A. Goddard III *J. Phys. Chem. A 105* **2001** 9396-9409

[12] W. J. Mortier, S. K. Ghosh, and S. Shankar *J. Am. Chem. Soc. 108* **1986** 4315

[13] G. O. A. Janssens, B. G. Baekelandt, H. Toufar, W. J. Mortier, R. A. Schoonheydt *J. Phys. Chem. 99* **1995** 3251

[14] P. Hohenberg and W. Kohn *Phys. Rev. B 136* **1964** 864

[15] K. Burke and friends, The ABC of DFT *http://dft.uci.edu/book/gamma/g1.pdf* **2007** 58

[16] A. R. Leach, Molecular modelling principles and applications second ed. *Oxford University Press, Oxford* **2001** 129, eq 3.46

[17] R. G. Parr, Density-functional theory of atoms and molecules *Oxford University Press, Oxford* **1994** 16, eq 1.6.1

[18] A. R. Leach, Molecular modelling principles and applications second ed. *Pearson Education Limited, Harlow* **2001** 38-41

[19] R. G. Parr, Density-functional theory of atoms and molecules *Oxford University Press, Oxford* **1994** 15, eq 1.5.6

[20] R. G. Parr, Density-functional theory of atoms and molecules *Oxford University Press, Oxford* **1994** 47, eq 3.1.1

[21] A. R. Leach, Molecular modelling principles and applications second ed. *Pearson Education Limited, Harlow* **2001** 49-50, eq 2.110

[22] W. J. Carr and A. A. Maradudin *Phys. Rev. A 133* **1964** 371

[23] C. Adamo and V. Barone *J. Chem. Phys. 116* **2002** 5933

[24] K. Burke and friends, The ABC of DFT *http://dft.uci.edu/book/gamma/g1.pdf* **2007** 90

[25] J. P. Perdew, K. Burke, and Y. Wang *Phys. Rev. B 54* **1996** 16533

[26] S. J Vosko, L. Wilk, and M. Nusair *Can. J. Phys. 58* **1980** 1200

[27] D. M. Ceperley and B. J. Alder *Phys. Rev. Lett.* **1980** 566

[28] J. P. Perdew and Y. Wang *Phys. Rev. B 45* **1992** 13244

[29] A. D. Becke *Phys. Rev. A 33* **1988** 3098

[30] C Lee, W Yang, and R. G. Parr *Phys. Rev. B 37* **1988** 785

[31] Colle and O. Salvetti *Theor. Chim. Acta 37* **1975** 329

[32] J. P. Perdew, K. Burke and M. Ernzerhof *Phys. Rev. Lett. 77* **1996** 3865

[33] B. Hammer, L. B. Hansen and J. K. Nørskov *Phys. Rev. B 59* **1999** 7413

[34] P. C. Hemmer, Kvantemekanikk *Tapir, Trondheim* **2000** 353, eq 17.26

[35] P. C. Hemmer, Kvantemekanikk *Tapir, Trondheim* **2000** 355, eq 17.39

[36] J. C. Slater *Phys. Rev. 36* **1930** 57

[37] A. R. Leach, Molecular modelling principles and applications second ed. *Oxford University Press, Oxford* **2001** 65, eq 2.188

[38] W. Kohn, and L. J. Sham *Phys. Rev. A 140* **1965** 1133

[39] U. von Barth and C. D. Gelatt *Phys. Rev. B 21* **1980** 2222

[40] *http://www.notur.no/hardware/njord/*

[41] *http://www.notur.no/hardware/stallo/*

[42] Scientific Computing & Modelling *http://www.scm.com/*

[43] E. van Lenthe, E. J. Baerends, Optimized Slater-Type Basis Sets for the Elements 1-118 *J. Comput. Chem. 24* **2002** 1142

[44] K. T. Olsen, Master assignment *Department of Physics, NTNU, Norway* **July 2009**

[45] *http://cst-www.nrl.navy.mil/lattice/struk/l1_.html*

A   Crystal structures with corresponding primitive and basis vectors

The figures of B_1, B_2, $l1_0$, CP, PP, α and are found from Ref. [45].
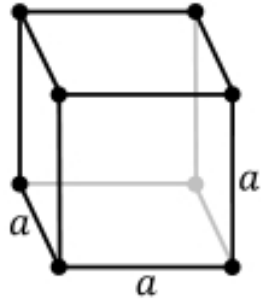
Figure 23: Simple cubic SC.

Figure 24: Body centered cubic BCC.

The primitive vectors for SC are
$$\vec{A}_1 = a\vec{x}$$
$$\vec{A}_2 = a\vec{y}$$
$$\vec{A}_3 = a\vec{z}$$
And the basis vectors are
$$C_1 : \vec{B}_1 = 0$$

The primitive vectors for BCC are
$$\vec{A}_1 = -\tfrac{1}{2}a\vec{x} + \tfrac{1}{2}a\vec{y} + \tfrac{1}{2}a\vec{z}$$
$$\vec{A}_2 = \tfrac{1}{2}a\vec{x} - \tfrac{1}{2}a\vec{y} + \tfrac{1}{2}a\vec{z}$$
$$\vec{A}_3 = \tfrac{1}{2}a\vec{x} + \tfrac{1}{2}a\vec{y} - \tfrac{1}{2}a\vec{z}$$
And the basis vectors are
$$C_1 : \vec{B}_1 = 0$$
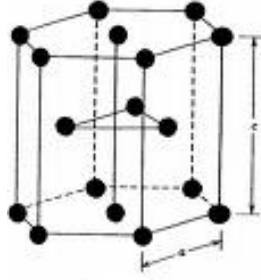
Figure 25: Hexagonal close packed lattice *HCP*.

The primitive vectors for *HCP* are
$\vec{A}_1 = \frac{1}{2}a\vec{x} - \frac{1}{2}3^{1/2}a\vec{y}$
$\vec{A}_2 = \frac{1}{2}a\vec{x} + \frac{1}{2}3^{1/2}a\vec{y}$
$\vec{A}_3 = c\vec{z}$
And the basis vectors are
$C_1 : \vec{B}_1 = \frac{1}{2}a\vec{x} + \frac{1}{2}3^{1/2}a\vec{y} + \frac{1}{4}c\vec{z}$
$C_1 : \vec{B}_2 = \frac{1}{2}a\vec{x} - \frac{1}{2}3^{1/2}a\vec{y} + \frac{3}{4}c\vec{z}$
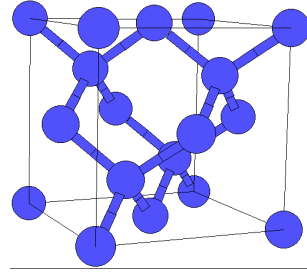
Figure 26: Cubic diamond structure, *diamond*.

The primitive vectors for cubic *diamond* are
$\vec{A}_1 = \frac{1}{2}a\vec{y} + \frac{1}{2}a\vec{z}$
$\vec{A}_2 = \frac{1}{2}a\vec{x} + \frac{1}{2}a\vec{z}$
$\vec{A}_3 = \frac{1}{2}a\vec{x} + \frac{1}{2}a\vec{y}$
And the basis vectors are
$C_1 : \vec{B}_1 = 0$
$C_1 : \vec{B}_2 = \frac{1}{4}a\vec{x} + \frac{1}{4}a\vec{y} + \frac{1}{4}a\vec{z}$
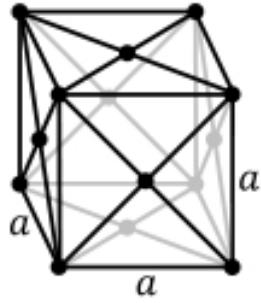
Figure 27: Face centered cubic FCC.

Figure 28: $B1$ structure.

The primitive vectors for FCC are
$\vec{A}_1 = \frac{1}{2}a\vec{y} + \frac{1}{2}a\vec{z}$
$\vec{A}_2 = \frac{1}{2}a\vec{x} + \frac{1}{2}a\vec{z}$
$\vec{A}_3 = \frac{1}{2}a\vec{x} + \frac{1}{2}a\vec{y}$
And the basis vectors are
$C_1 : \vec{B}_1 = 0$

The primitive vectors for $B1$ are
$\vec{A}_1 = \frac{1}{2}a\vec{y} + \frac{1}{2}a\vec{z}$
$\vec{A}_2 = \frac{1}{2}a\vec{x} + \frac{1}{2}a\vec{z}$
$\vec{A}_3 = \frac{1}{2}a\vec{x} + \frac{1}{2}a\vec{y}$
And the basis vectors are
$C_1 : \vec{B}_1 = 0$
$C_2 : \vec{B}_2 = \frac{1}{2}a\vec{x} + \frac{1}{2}a\vec{y} + \frac{1}{2}a\vec{z}$

72
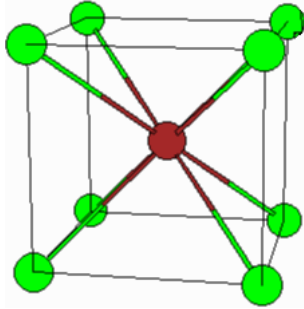
Figure 29: $B2$ structure.

Figure 30: Cubic $l1_0$ structure, $l1_0$.

The primitive vectors for $B2$ are
$\vec{A_1} = a\vec{x}$
$\vec{A_2} = a\vec{y}$
$\vec{A_3} = a\vec{z}$
And the basis vectors are
$C_1 : \vec{B_1} = 0$
$C_2 : \vec{B_2} = \frac{1}{2}a\vec{x} + \frac{1}{2}a\vec{y} + \frac{1}{2}a\vec{z}$
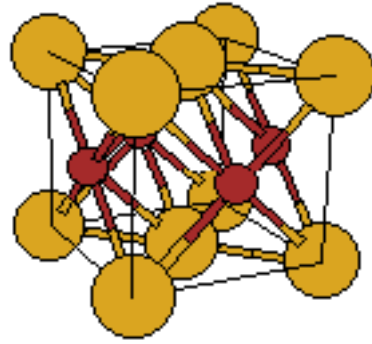
The primitive vectors for cubic $l1_0$ are
$\vec{A_1} = \frac{1}{2}a\vec{x} - \frac{1}{2}a\vec{y}$
$\vec{A_2} = \frac{1}{2}a\vec{x} + \frac{1}{2}a\vec{y}$
$\vec{A_3} = a\vec{z}$
And the basis vectors are
$C_1 : \vec{B_1} = 0$
$C_2 : \vec{B_2} = \frac{1}{2}a\vec{x} + \frac{1}{2}a\vec{z}$
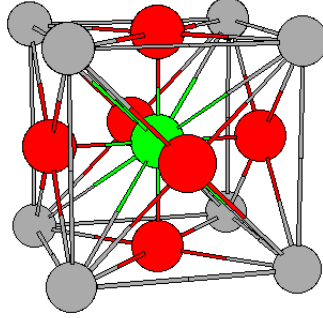
Figure 31: Cubic perovskite lattice CP.

The primitive vectors for CP are
$\vec{A}_1 = a\vec{x}$
$\vec{A}_2 = a\vec{y}$
$\vec{A}_3 = a\vec{z}$
And the basis vectors are
$C_1 : 0$
$C_2 : \vec{B}_1 = \frac{1}{2}a\vec{y} + \frac{1}{2}a\vec{z}$
$C_2 : \vec{B}_2 = \frac{1}{2}a\vec{x} + \frac{1}{2}a\vec{z}$
$C_2 : \vec{B}_3 = \frac{1}{2}a\vec{x} + \frac{1}{2}a\vec{y}$
$C_3 : \frac{1}{2}a\vec{x} + \frac{1}{2}a\vec{y} + \frac{1}{2}a\vec{z}$
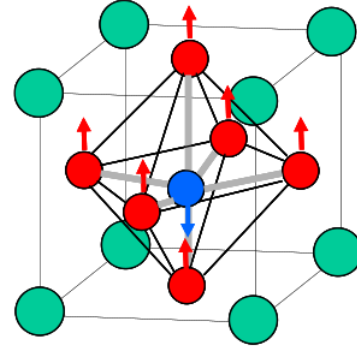
Figure 32: Polarized perovskite lattice PP.

The δ_1, δ_2, and δ_3, are displacements in the z direction in comparison to a tetragonal perovskite structure. The primitive vectors for PP are
$\vec{A}_1 = a\vec{x}$
$\vec{A}_2 = a\vec{y}$
$\vec{A}_3 = c\vec{z}$
And the basis vectors are
$C_1 : 0$
$C_2 : \vec{B}_1 = \frac{1}{2}a\vec{y} + \frac{1}{2}c\vec{z} + \delta_1\vec{z}$
$C_2 : \vec{B}_2 = \frac{1}{2}a\vec{x} + \frac{1}{2}c\vec{z} + \delta_1\vec{z}$
$C_2 : \vec{B}_3 = \frac{1}{2}a\vec{x} + \frac{1}{2}\vec{y} + \delta_2\vec{z}$
$C_3 : \vec{B}_4 = \frac{1}{2}a\vec{x} + \frac{1}{2}a\vec{y} + \frac{1}{2}c\vec{z} + \delta_3\vec{z}$
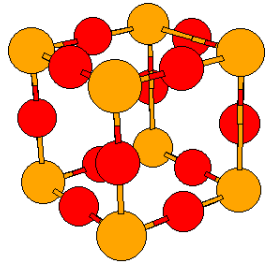
Figure 33: The cubic α lattice.

The primitive vectors for cubic α are
$\vec{A}_1 = a\vec{x}$
$\vec{A}_2 = a\vec{y}$
$\vec{A}_3 = a\vec{z}$
And the basis vectors are
$C_1 : 0$
$C_2 : \vec{B}_1 = \frac{1}{2}a\vec{x}$
$C_2 : \vec{B}_2 = \frac{1}{2}a\vec{y}$
$C_2 : \vec{B}_3 = \frac{1}{2}a\vec{z}$

B Plots for bond stretches, valence angles, and torsion angles

This appendix contains plots for all results for bond stretches, valence angles, and torsion angles. It is the atom that is not hydrogen that is relevant to the distance, valence angle, or torsion angle. I.e. for the distance PbH_3-PbH_3, it is the two lead atoms the distance is measured between.
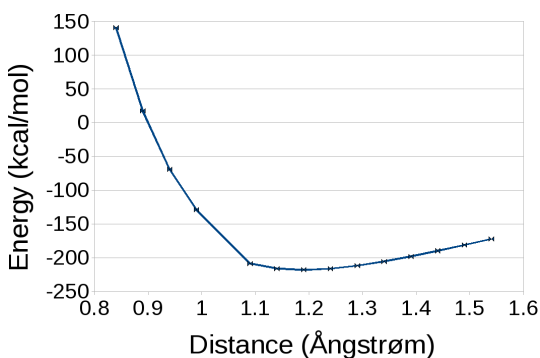
Figure 34: Energy as a function of the distance O-O in O_2. The molecule is illustrated in Fig. 56

Figure 35: Energy as a function of the Pb-O distance in PbH_2O. The molecule is illustrated in Fig. 57. The energy drop at 2.5 Å is because the geometry changes from being in a local energy minimum to another, more stable energy minimum.

Figure 36: Energy as a function of the O-O distance in OHOH. The molecule is illustrated in Fig. 55.
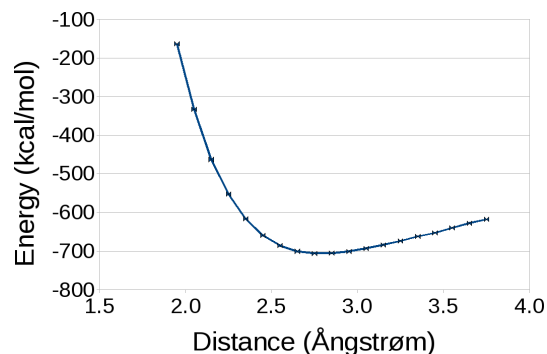
Figure 37: Energy as a function of the Pb-Ti distance in PbTi. The molecule is illustrated in Fig. 58.
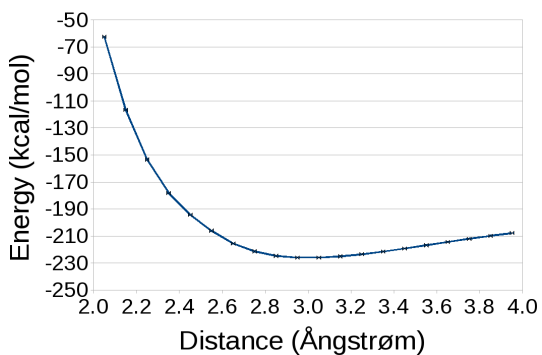
Figure 38: Energy as a function of the Pb-Pb distance in Pb_2. The molecule is illustrated in Fig. 61.
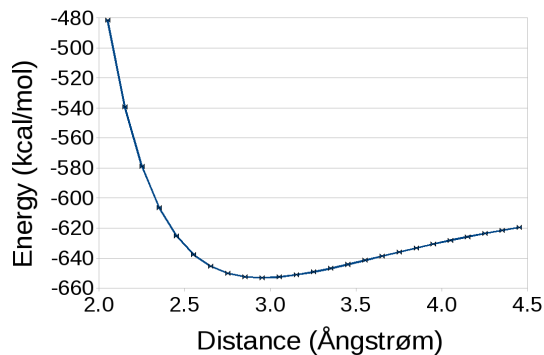
Figure 39: Energy as a function of the Pb-Pb distance in PbH_3PbH_3. The molecule is illustrated in Fig. 60.
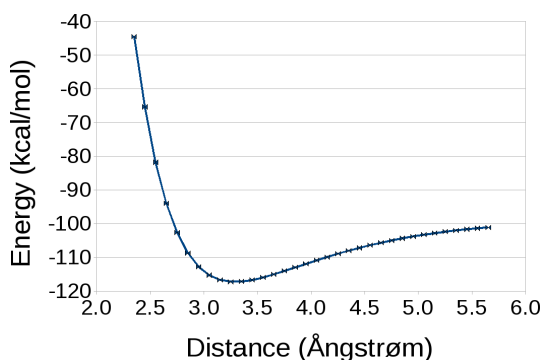
Figure 40: Energy as a function of the Pb-Sr distance in PbSr. The molecule is illustrated in Fig. 72.
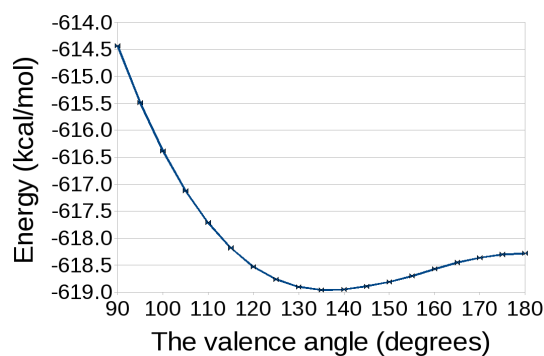
Figure 41: Energy as a function of the Pb-Sr-O valence angle in PbH_3SrOH. The molecule is illustrated in Fig. 62.
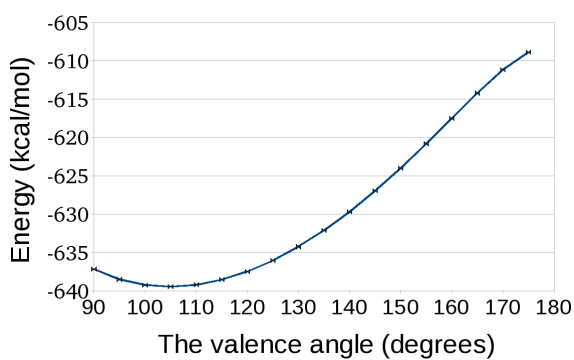
Figure 42: Energy as a function of the Pb-O-O valence angle in PbH$_3$OOH. The molecule is illustrated in Fig. 66.
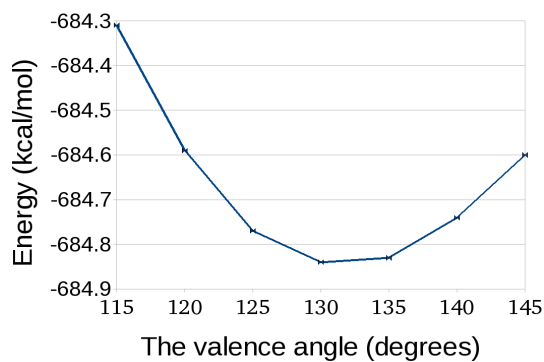
Figure 43: Energy as a function of the Pb-Sr-Pb valence angle in PbH$_3$SrPbH$_3$. The molecule is illustrated in Fig. 63.
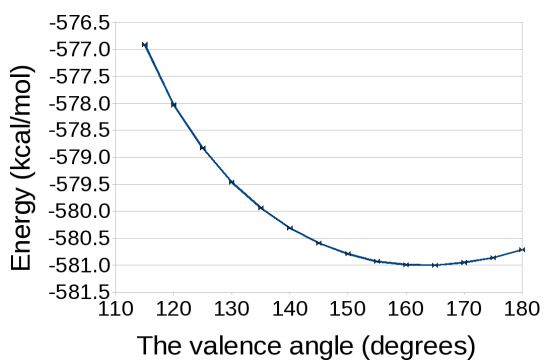
Figure 44: Energy as a function of the Pb-O-Sr valence angle in PbH$_3$OSrH. The molecule is illustrated in Fig. 64.
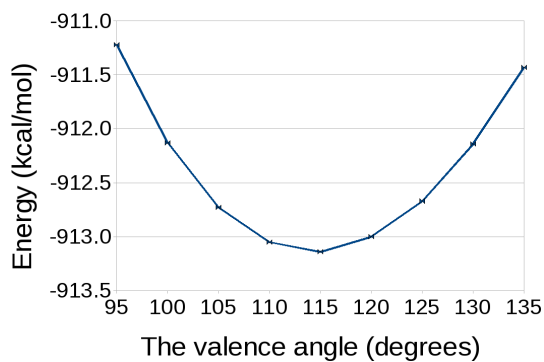
Figure 45: Energy as a function of the Pb-Pb-Pb valence angle in PbH$_3$PbH$_2$PbH$_3$. The molecule is illustrated in Fig. 68.
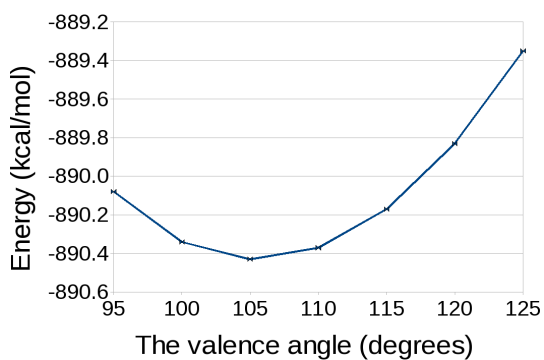
Figure 46: Energy as a function of the Pb-Ti-Pb valence angle in $PbH_3TiH_2PbH_3$. The molecule is illustrated in Fig. 65.
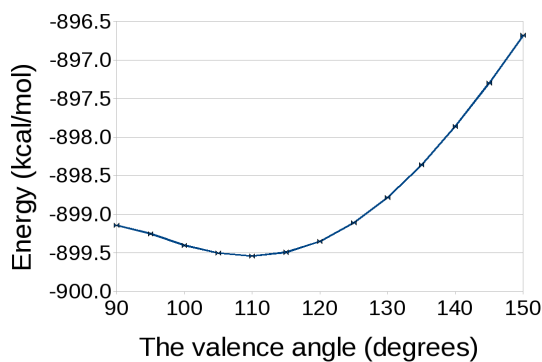
Figure 47: Energy as a function of the Pb-Pb-Ti valence angle in $PbH_3PbH_2TiH_3$. The molecule is illustrated in Fig. 69.
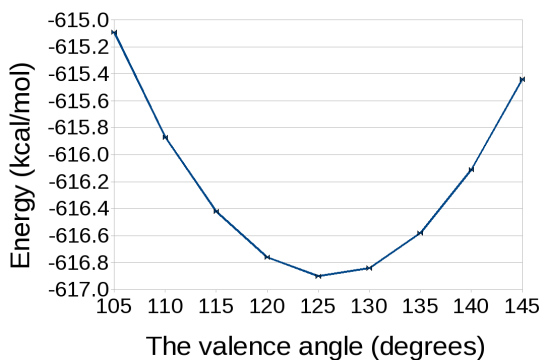
Figure 48: Energy as a function of the Pb-Pb-O valence angle in PbH_3PbHO. The molecule is illustrated in Fig. 67.
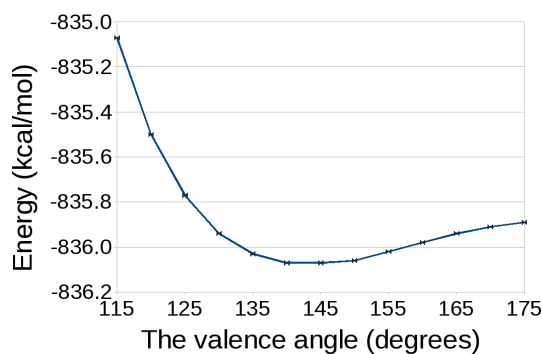
Figure 49: Energy as a function of the Pb-O-Ti valence angle in PbH_3OTiH_3. The molecule is illustrated in Fig. 70.
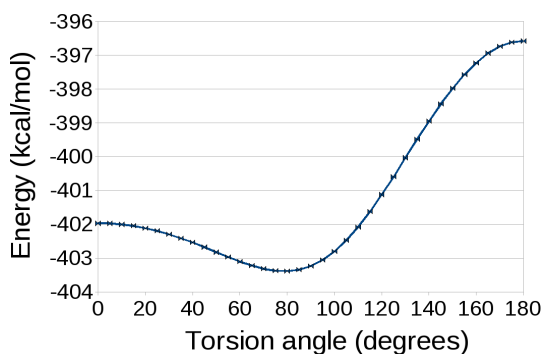
Figure 50: Energy as a function of the H-O-O-H torsion angle in OHOH. The molecule is illustrated in Fig. 55, and the molecular structure implies that $E(\theta) = E(-\theta)$
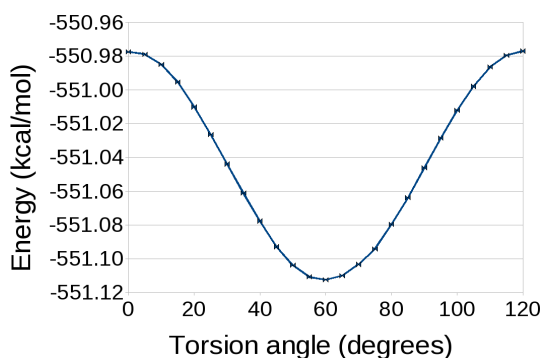
Figure 51: Energy as a function of the H-Pb-O-H torsion angle in PbH_3OH. The geometry of the molecule, illustrated in Fig. 71, implies that $E(\theta) = E(-\theta)$, and that the energy is periodic with a period of 120 degrees.
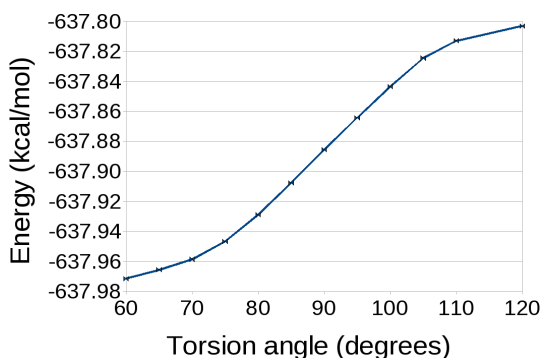
Figure 52: Energy as a function of the H-Pb-Ti-H torsion angle in PbH_3TiH_3. The geometry of the molecule, illustrated in Fig. 73, implies that $E(\theta) = E(-\theta)$, and that the energy is periodic with a period of 120 degrees.
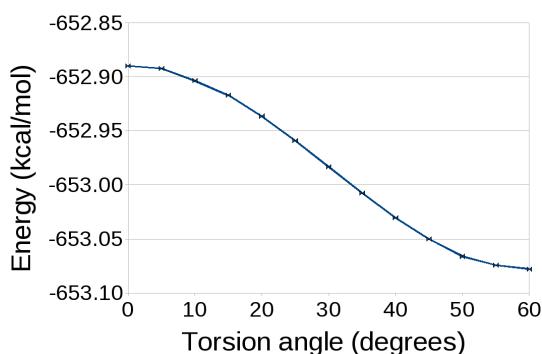
Figure 53: Energy as a function of the H-Pb-Pb-H torsion angle in PbH_3PbH_3. The geometry of the molecule, illustrated in Fig. 59, implies that $E(\theta) = E(-\theta)$, and that the energy is periodic with a period of 120 degrees
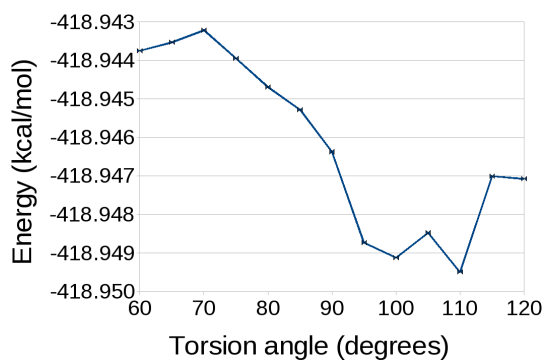
Figure 54: Energy as a function of the H-Pb-Sr-H torsion angle in PbH$_3$SrH. The uneven plot is due to numerical errors. The geometry of the molecule, illustrated in Fig. 60, implies that $E(\theta) = E(-\theta)$, and that the energy is periodic with a period of 120 degrees.

C   Molecules used in the computations
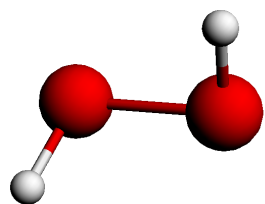
Figure 55: The OHOH molecule.
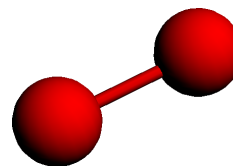
Figure 56: The O$_2$ molecule.
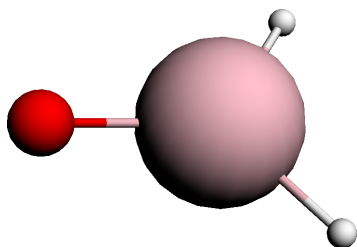
Figure 57: The PbH$_2$O molecule.
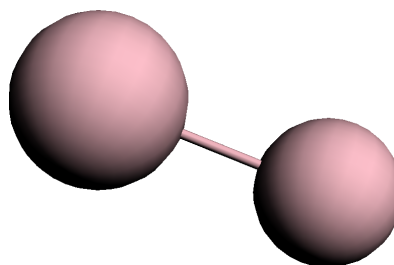
Figure 58: The PbTi molecule.

81
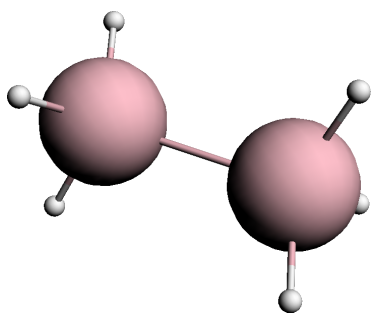
Figure 59: The PbH$_3$PbH$_3$ molecule.
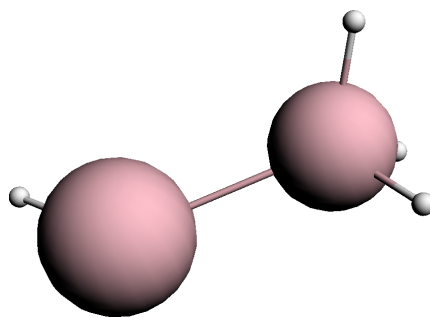
Figure 60: The PbH$_3$SrH molecule.
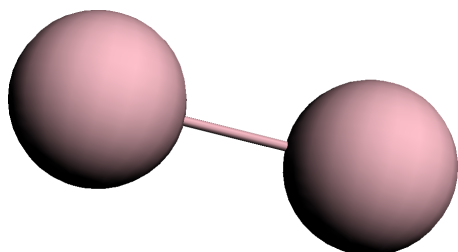
Figure 61: The Pb$_2$ molecule.
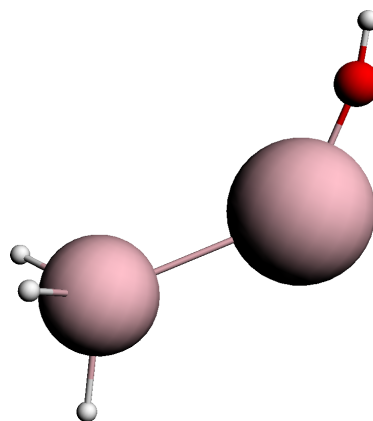
Figure 62: The PbH$_3$SrOH molecule. The atom to the left is Pb, bound to 3 hydrogen atoms and a Sr atom.
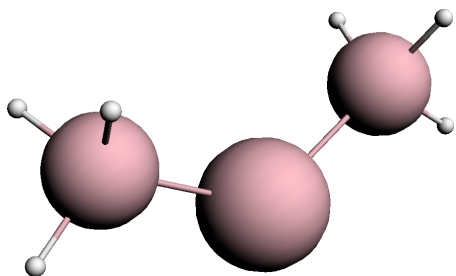
Figure 63: The PbH$_3$SrPbH$_3$ molecule.
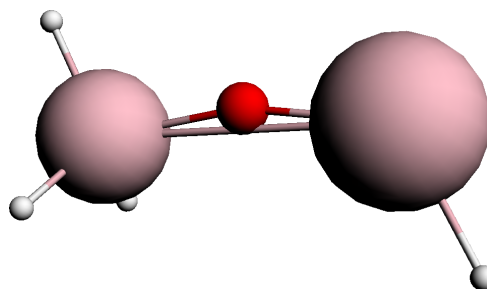
Figure 64: The PbH$_3$OSrH molecule. The atom to the left is Pb, O is in the middle, and Sr is the atom to the right.
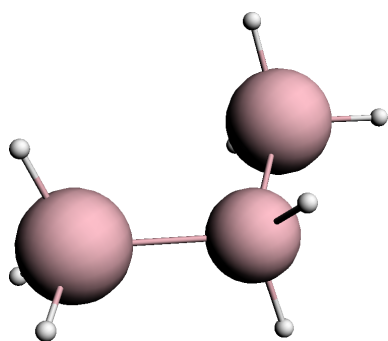
Figure 65: The PbH$_3$TiH$_2$PbH$_3$ molecule.
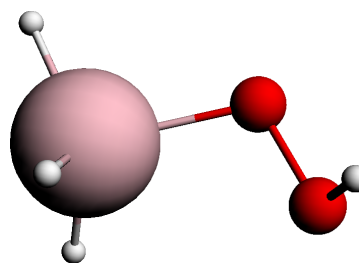
Figure 66: The PbH$_3$OOH molecule.
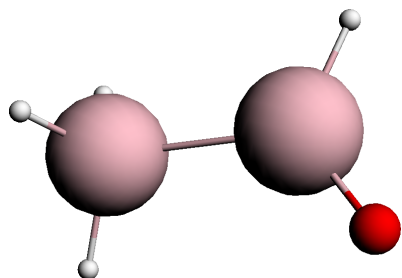
Figure 67: The PbH$_3$PbHO molecule.
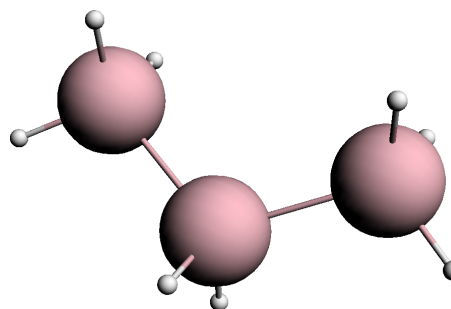
Figure 68: The PbH$_3$PbH$_2$PbH$_3$ molecule.
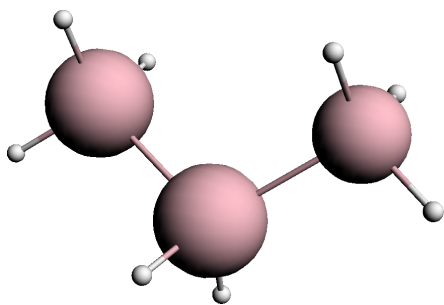
Figure 69: The PbH$_3$PbH$_2$TiH$_3$ molecule. The atom to the right is Ti.
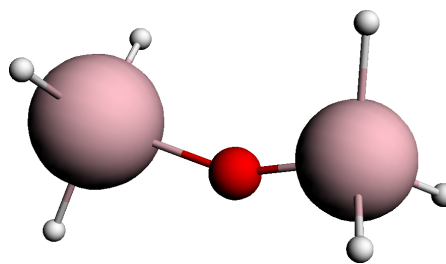
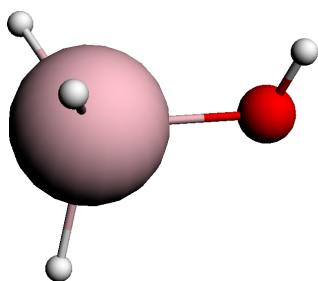Figure 70: The PbH$_3$OTiH$_3$ molecule.

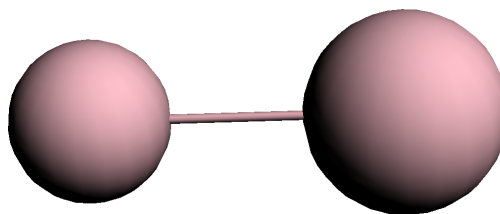Figure 71: The PbH$_3$OH molecule.
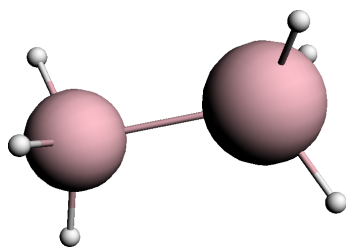

Figure 72: The PbSr molecule.

Figure 73: The PbH$_3$TiH$_3$ molecule. The largest atom is Pb.